A DESIGN-ORIENTED FRAMEWORK TO DETERMINE THE PARASITIC PARAMETERS OF HIGH FREQUENCY MAGNETICS IN SWITCING POWER SUPPLIES USING FINITE ELEMENT ANALYSIS TECHNIQUES

A Thesis

by

MOHAMMAD BAGHER SHADMAND

Submitted to the Office of Graduate Studies of
Texas A&M University
in partial fulfillment of the requirements for the degree of

MASTER OF SCIENCE

May 2012

Major Subject: Electrical Engineering

A Design-Oriented Framework to Determine the Parasitic Parameters of High Frequency Magnetics in Switching Power Supplies using Finite Element Analysis Techniques

A DESIGN-ORIENTED FRAMEWORK TO DETERMINE THE PARASITIC PARAMETERS OF HIGH FREQUENCY MAGNETICS IN SWITCING POWER SUPPLIES USING FINITE ELEMENT ANALYSIS TECHNIQUES

A Thesis

by

MOHAMMAD BAGHER SHADMAND

Submitted to the Office of Graduate Studies of
Texas A&M University
in partial fulfillment of the requirements for the degree of

MASTER OF SCIENCE

Approved by:

Chair of Committee,	Robert S. Balog
Committee Members,	Shankar P. Bhattacharyya
	Prasad Enjeti
	Theofanis Strouboulis
Head of Department,	Costas N. Georghiades

May 2012

Major Subject: Electrical Engineering

ABSTRACT

A Design-Oriented Framework to Determine the Parasitic Parameters of High Frequency Magnetics in Switching Power Supplies using Finite Element Analysis Techniques.

(May 2012)

Mohammad Bagher Shadmand, B.S., Qatar University

Chair of Advisory Committee: Dr. Robert S. Balog

Magnetic components, such as inductors and transformers, have important effects on the efficiency and performance of switching power supplies; their parasitic properties directly impact the high frequency properties which can cause lot-to-lot variation or unanticipated and non-ideal operation. They are also amongst the most problematic components to design, often requiring numerous design-prototype-test interactions. The electrostatic and electromagnetic analysis of wound components has become more important recently to predict their performance and frequency behavior.

Accurate prediction and design of winding parasitic parameters of leakage inductance and winding capacitance for high frequency inductors and transformers in switching power supplies is fundamental to improve performance, lower cost, and speed time to market. This thesis presents a methodology and process to obtain accurate prediction of the inter- and intra-winding capacitances of high frequency magnetic components. Application examples considered are a single-winding choke, a coupled inductor filter, and a multi-winding transformer. Analytical approach for determination

of parasitic capacitances in high frequency magnetic components will be covered also. Comparison of the FEA results using JMAG with experimental and empirical formula results show good agreement, supporting the method as a model-based design tool with the potential to significantly reduce the design-prototype-test cycle commonly needed with sophisticated magnetic designs.

DEDICATION

To my parents

ACKNOWLEDGEMENTS

I would like to thank my committee chair, Dr. Balog, and my committee members, Dr. Bhattacharyya, Dr. Enjeti, and Dr. Strouboulis, for their guidance and support throughout the course of this thesis.

Appreciations also go to my friends and colleagues and the department faculty and staff for making my time at Texas A&M University a great experience.

TABLE OF CONTENTS

Page

LIST OF FIGURES

Page

LIST OF TABLES

Page

1. INTRODUCTION

1.1 Statement of the problem and significance

Understanding and predicting parasitic winding capacitance in high frequency magnetic components is essential to improve the performance and efficiency of switch mode power supplies (SMPS). Magnetic components are one of the most significant components in power electronic devices, and arguably the most difficult to design-which gives rise to the "black magic" aspect of magnetic design. The fact that frequency affects the behavior of magnetic components is widely known [1]. Magnetic components such as transformers and inductors utilized in switch mode power supplies work with high frequency voltage and current waveforms. Moreover, these waveforms are typically nonsinusoidal, and they have a high harmonic content, which obliges the analysis of the behavior of magnetic components as a function of frequency. An accurate model helps to acquire accurate simulations of the electrical waveforms and the electromagnetic interferences (EMI). Consequently the design procedure of the entire SMPS is improved.

The resistance, inductance as well as capacitance of magnetic components depend on its geometry and operating frequency [2, 3]. Besides the losses and leakage inductance, a model should include the capacitive behavior. The modeling process must take into consideration the operating frequency and geometry of the component as a result the analysis becomes quite difficult especially for more complicated geometries

---

This thesis follows the style of *IEEE Transactions on Power Electronics*.

such as multi-winding transformers. More complex geometries indicate that it is almost impossible to derive the analytical equations that describe the behavior of magnetic components; therefore Finite Element Analysis (FEA) tools can be utilized to calculate the value of the parasitic parameters.

The design trend of better-faster-cheaper is driving miniaturization in power supplies. Smaller power supplies have to work at higher switching frequencies in order to condense size of the passive components which are a primary driver in the overall size and weight of the converter. Moreover, self-capacitances of transformers can be used as resonant elements in resonant DC-DC converters in order to reduce the overall system size [3]. In addition for the transformers within resonant converter where the switching frequency can rise up to 500 kHz [4], the parasitic parameters, as stray capacitances in particular, can deeply affect the performance of the converter. Furthermore, in order to predict the performance of the resonant converter and to be able to use the parasitic of the transformer as constitutive elements of the resonant circuit, the calculation of the stray capacitance is a fundamental issue. Besides it necessitates determining parasitic capacitance of the transformers without building the transformer physically which diminish the design test cycle.

The upper operating frequency of every coil and inductor is limited by its self-capacitance [5]. At high frequencies, the frequency response of a transformer is very different from its low frequency response [6, 7]. Unfortunately, above its first self-resonant frequency, an inductor or any other coils behaves like a capacitor. Figure 1 shows the common equivalent circuit of a single winding structure where L is the

inductance of the winding, R is the resistance of the winding, and C_s is the equivalent self-capacitance of the winding. At low frequency, self-capacitance, core losses, skin and proximity effects can be neglected [5, 8-10]. However, at high frequency, such as harmonics of the switching frequency, the equivalent circuit model fails to accurately capture the true performance.

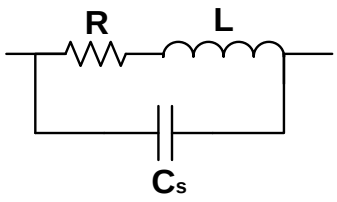

Figure 1: Equivalent electrical circuit for a winding

Therefore calculation of parasitic capacitances of magnetic components is fundamental for predicting the frequency behavior of the device, reducing these capacitances value and more advanced purposes of capacitance integration and cancellation.

1.2 Literature review

Within the literature, a lot of papers can be found dealing with modeling of losses and leakage inductances. Only a few papers discussed the capacitive effects of magnetic components comprehensively because of its complexity in some components. Pioneer investigations on methodologies for determination of the parasitic capacitances of magnetic components comes back to early 1930s [11, 12]. In these early works, Palermo investigated the approximate calculation of parasitic capacitance of a single layer coils

which are based on the experimental result, and his conclusion was that the distributed capacity of a single-layer coils depends mainly on the diameter of the winding and the ratio of pitch of winding to the diameter of bare wire.

In late 1980s and early 1990s several works has been done towards the electrostatic analysis of magnetic components [6, 7, 13-31], in these investigation multi-layer windings are also discussed. The most comprehensive work has been done by Massarini, his early works [6, 7] was focused mainly on predicting the stray capacitances of inductors. His methodology was based on an analytical approach and the physical structure of inductors, but he didn't take into consideration the frequency. His late 1990s paper [28] investigated a method for predicting parasitic capacitances of a high frequency single layer solenoid air-core inductors. In this work the method is also based on analytical approach to obtain the turn-to-turn and turn-to-shield capacitances of coils.

In the last decade more precise model of inter- and intra-winding capacitances of high frequency magnetic components have been investigated [1-3, 5, 8, 32-37]. Kolar and Biela [3] reviewed calculation methods of the stray capacitance of transformers, but they did not taken into consideration the turn-to-turn capacitances. Parasitic capacitance models of two-winding transformers are derived based on the static layer-to-layer capacitances. In some text books [9, 10] high frequency behaviors of magnetic components are discussed, but the self-capacitance of the windings are either missed in the models or derived based on empirical formulas for simple geometries such as single winding structures. So an accurate model based on all existing parasitic capacitances that can be applied any type of magnetic components geometries such the multi-winding

transformers which are commonly utilized in switch mode power supplies is missed in literature.

Recently by developing the FEA tool packages it is become possible to propose a methodology that can predict accurately intra- and inter-winding capacitances of magnetic components which take into consideration physical properties and frequency. However the analytical approaches presented in literature may be useful for simple geometries such as single winding structures and two-winding transformers, but as the geometry becomes more complicated the analytical methods are insufficient and a design-oriented framework by means of FEA tool is needed which is the main goal of this thesis. Therefore FEA tools approach are a good tradeoff between speed to obtain results and their accuracy.

1.3 Organization of the thesis and portions which have previously been published

This thesis is organized as follows. The methodology which includes the theoretical backgrounds on determination of parasitic capacitances of magnetic components by means of FEA is discussed in chapter 2. The first application which is the single winding structure and is utilized to propose a methodology for determination of parasitic capacitances by means of FEA tool, JMAG is discussed in chapter 3. The third and fourth chapters are dedicated to coupled inductor filters and multi-winding transformers application respectively which have more complicated geometry than the previously mentioned application. The developed method in chapter 2 is utilized for determining the parasitic capacitances in coupled inductors and multi-winding

transformers. Finally future work and conclusion are discussed in chapter 6 and 7 respectively.

Some sections of this thesis is published and/or submitted for peer review [38-40]. The coupled inductor application, presented in chapter 4, submitted for peer review and accepted to be published [38]. Application of single winding magnetic components, presented in chapter 3, to improve the performance, manufacturability, and efficiency of photovoltaic inverters is submitted for peer review [40].

2. METHODOLOGY

2.1 Self-capacitance components

The self-capacitance models the parasitic capacitive coupling between the terminals of the winding of a transformer or any other coil. This capacitance allows the current to flow directly from one terminal to the other without passing through the inductance [10]. The main contributions to the self-capacitance in a high frequency transformer are the following [5, 10]:

a) The turn-to-turn capacitance within the same layer
b) The layer to layer capacitance
c) Winding to magnetic core capacitance
d) Intertwining interactions

The self-capacitance is highly dependent on the winding geometry and the proximity of conducting surfaces [18]. The distributed turn-to-turn behaves like a shunt capacitance, conducting a high frequency current [10]. The following three factors are the main factors that affect the value of the self-capacitance [3, 5]:

a) The winding arrangement and the strategy of connecting the different winding sections which thus affect the amount of the electrostatic energy stored as it is shown in Figure 2

b) The dielectric constant of the insulating materials interposed between the layers

c) The geometry model such as diameter and dimension of the energized conductor, and the mutual spacing between wires and their distance to the core

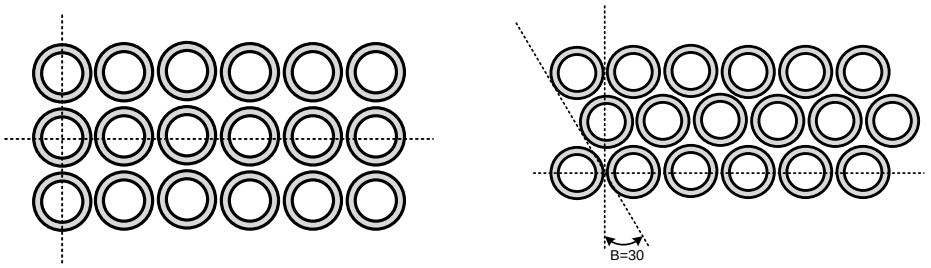

Figure 2: Arrangements of turns: (a) conductors aligned and (b) hexagonal turns grid

In addition to the above mentioned parameters in the ferrite core components, the resonant properties of the ferrite material itself can also increase the apparent equivalent intra capacitance. Two conductors with a surface charge ρ_s and a potential difference between the conductors V, then by using the Gauss's law, the charged stored in the conductor is [4]:

$$Q = \oint_S \rho_s dS = \oint_S \epsilon E.ds \quad (1)$$

The voltage between the conductors is

$$V = -\int_{P_1}^{P_2} E.dl \quad (2)$$

Where P_1 is a point located on the conductor with –Q and P_2 is a point located on conductor with + Q. Therefore the capacitance of two conductors can be calculated as following:

$$C = \frac{Q}{V} = \frac{\oint_S \epsilon E.ds}{-\int_{P_1}^{P_2} E.dl} \quad (3)$$

2.2 FEA theory and methodology

2.2.1 Inter-winding capacitance

The inter-winding capacitance usually generates common mode currents in galvanic insulated converters. It is also a matter of safety to obtain low common mode currents, especially in medical equipment [9]. The inter-winding capacitance can be demonstrated as:

$$C_{inter} = \frac{\varepsilon_0 \varepsilon_r S}{d} \quad (4)$$

Where:
S is the area between the windings
ε_0 is the permittivity of the air
ε_r is the relative permittivity
d is the distance between the wires of adjacent layers

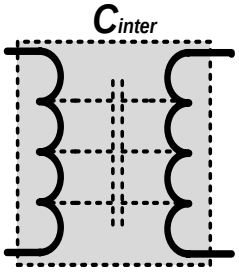

Figure 3: Inter-winding capacitance of two arbitrary winding in a transformer

By applying a voltage to a winding for excitation, the total charge can be calculated depending on the voltages between adjacent surfaces, so:

$$Q = \int (V' - V'') \varepsilon_0 \varepsilon_r \frac{dS}{d} \quad (5)$$

$$V_{eq} = \frac{Q}{C_{inter}}$$

Where:

$V' - V''$ is the voltage between adjacent wires of different layers
dS is an elementary surface

2.2.2 Parallel plate capacitor model

One of the common methods for determining the layer-to-layer static capacitance in case of multi-layer winding structure is called parallel plate capacitor model, the main principle of this method is to replace the wound wires by flat rectangles, as shown in Figure 4. The second step is to replace the flat rectangles by an equipotential surface as shown in Figure 4 [3], the d_{eff} is the effective distance between the plates. It can be calculated by determining the capacitance of the real arrangement of the wires, the capacitance of the two wire grids and the value of the parallel plate capacitor. By equating these two capacitances the value of d_{eff} can be calculated as:

$$d_{eff} = d' - 2.3 \times (r_0 + \delta) + 0.26 \times d_{tt} \tag{6}$$

$$d' = d = 2 \times r_0 + h \qquad for\ orthogonal\ structure \tag{7}$$

$$d' = \begin{cases} d = 2r_0 + h & if\ h > 0 \\ r_0 + \frac{h}{2} + \frac{\sqrt{(2r_0+h)^2 + \frac{d_{tt}^2}{4}}}{2} & if\ h \leq 0 \end{cases} \qquad for\ orthocyclic\ structure \tag{8}$$

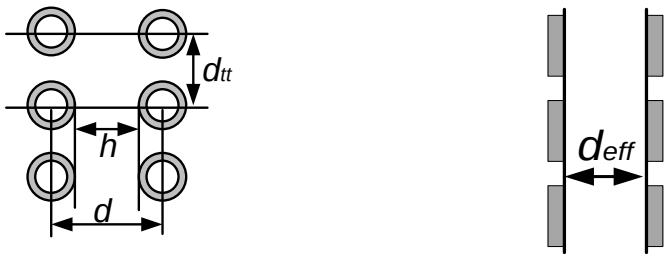

(a) (b)

Figure 4: a) orthogonal winding b) effective distance definition

The value of the parallel-plate capacitor could be calculated as [3]:

$$C_{parallel-plate} = \varepsilon_0 \varepsilon_{r,m} \frac{l_{w,m} L_L}{d_{eff}} \quad (9)$$

$$\varepsilon_{r,m} = \frac{\varepsilon_D \varepsilon_F (\delta + h)}{\varepsilon_F \delta + \varepsilon_D h},\ h = R_{2,cyl} - R_{1,cyl}\ ,\ l_{w,m} = \pi(R_{1,cyl} + R_{2,cyl}) \quad (10)$$

The effective permittivity, $\varepsilon_{r,m}$, can be determined by equating the voltage across the series connected dielectrics and the voltage across the equivalent dielectrics or by equating the stored energies [3, 5, 9].

2.2.3 Cylindrical capacitor model

Some of the windings have a cylindrical shape, in this modeling configuration; the parallel plate capacitor will be replaced by a cylindrical capacitor. Thus, the round wires of a layer have been replaced by equipotential surface, as a result the capacitance can be calculated as [3]:

$$C_{Cylindrical-Cap} = \frac{\varepsilon_0 \varepsilon_{r,m} 2\pi L_L}{ln\left(\frac{R_{1,cyl} + d_{eff}}{R_{1,cyl}}\right)} \quad (11)$$

$$R_{1,cyl} = \frac{R_{L1} + R_{L2} - d_{eff}}{2} \quad (12)$$

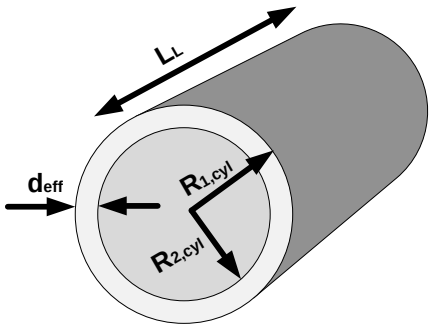

Figure 5: Cylindrical capacitor model of two successive layer of the winding

In high frequency and high power magnetic components the difference between the parallel plate and cylindrical capacitor model is very small so the simpler parallel

plate capacitor model can be used in most of the case specially for complicated geometries such as multilinking transformers [3, 5, 9, 41]. There are several other analytical models which are based on the approximation of the electric flux lines by straight lines which can be approximated with a FEA tool, these methods will be used in simulation chapter of this study for determining the equivalent self-capacitance of the winding's lumped capacitor network.

2.3 Turn-to-turn capacitance calculation

The first step to calculate the self-capacitance of a single layer winding is to find the turn-to-turn capacitance, different methods for scheming turn-to-turn capacitance analytically and empirically has been reviewed in the literature [3, 5-8, 15, 32], this capacitance between two individual turns can be calculated as following when the insulation coating is neglected, cross section two individual turn of a conductor shown in Figure 3:

$$C_{tt} = \frac{\pi \epsilon l_T}{cosh^{-1}\left(\frac{P}{2a}\right)} = \frac{\pi \epsilon l_T}{\ln\left[\frac{p}{2a}+\sqrt{\left(\frac{p}{2a}\right)^2-1}\right]} = \frac{\pi^2 \epsilon D_T}{\ln[\frac{p}{2a}+\sqrt{\left(\frac{p}{2a}\right)^2-1}]}, \quad for \;\; t \ll p-2a \tag{13}$$

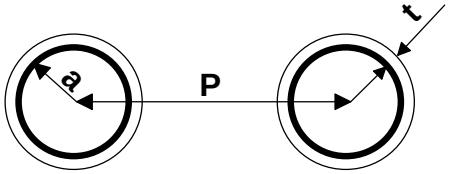

Figure 6: Cross section of two individual adjacent turns

The capacitance of cylindrical capacitor with two insulating layer can be used to determine the turn-to-turn capacitance with insulation coating of thickness t, therefore

the equivalent turn-to-turn capacitance is equal to the series combination of capacitance related to air gap and insulation coating between two adjacent turns. The C_{tt} related to air gap between two adjacent turns is given by:

$$C_g = \frac{\pi \epsilon_0 l_T}{ln\left[\frac{p/_{2a}}{1+\frac{t}{a}} + \sqrt{\left(\frac{p/_{2a}}{1+\frac{t}{a}}\right)^2 - 1}\right]} \tag{14}$$

$$C_{tt} = \frac{\pi^2 \epsilon_0 D_T}{ln\left\{\left[\frac{p/_{2a}}{(1+\frac{t}{a})^{1-\frac{1}{\epsilon_r}}}\right] + \sqrt{\left(\frac{p/_{2a}}{(1+\frac{t}{a})^{1-\frac{1}{\epsilon_r}}}\right)^2 - \left(1+\frac{t}{a}\right)^{2/\epsilon_r}}\right\}} \tag{15}$$

2.4 Layer-to-layer capacitance

2.4.1 General approach

Practically by using the C_{tt} determined in previous sections the value of the capacitance between two layers of turns can be calculated as following:

$$C_{ll} = \frac{n_t(n_t+1)(2n_t+1)}{6n_t^2} l C_{tt} \tag{16}$$

Where n_t is the number of turns and l is the average length of a turn.

Using above equation to determine the layer-to-layer capacitance is worthwhile if the number of turns are less than 10, but for larger number of turns it is suggested [5, 37, 41] to use the following formula for determination of layer-to layer capacitance if the curvature radius *r* is large of a parallel plate capacitor model:

$$C_{ll} = \varepsilon_0 \varepsilon_r \frac{2\pi\omega}{\ln(1+\frac{d}{r})} \quad if\ r \to \infty\ C_{ll} = \varepsilon_0 \varepsilon_r \frac{2\pi r \omega}{\mathrm{d}} \tag{17}$$

Where d is the distance between two adjacent layers and ω is the width of a layer.

The value of *d* is not provided by two times the insulation thickness, but is usual to use some empirical formulas as mentioned in literature [5, 12] to determine this distance:

$$d = 1.26 \times d_e - 1.15 \times d_i \quad (18)$$

d_e and d_i: are external and internal wire diameters respectively

In order to have a very accurate results for using the above equation the insulation shouldn't be thick, if the insulation of the wires are thick the actual distribution of the flux lines can be more complex, therefore accurate information of wire's characteristics such its insulation thickness and cross section are needed. The static capacitance C_{ll} derived base on the assumption of uniform charge distribution over conductors of each layer disconnected, but this value will be changed base on the connection configurations of adjacent layers.

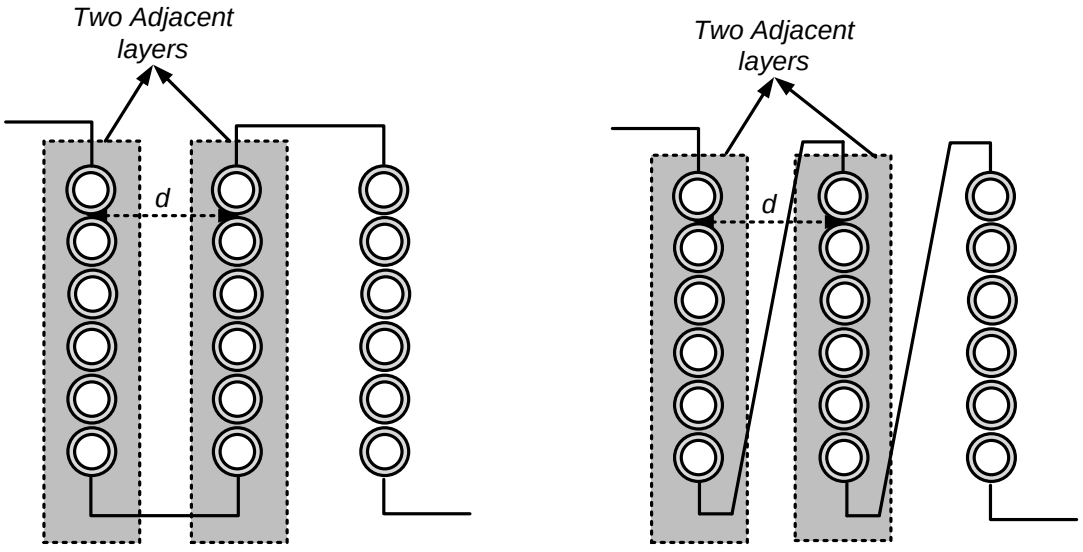

Figure 7: Multi-layer winding configuration a) multi-layer standard b) multi-layer flyback

"Principle of Virtual Work" (PVW) is one of the ways to determine the equivalent capacitance when different connections of layers are considered. If *V* is the voltage between two layers then the corresponding electrostatic energy $W\epsilon$ stored between the layers is given by:

$$W_\varepsilon = \frac{1}{2}\int_{Vol} D.Edv = \frac{1}{2}C_{ll}V^2 \quad (19)$$

The electric field base on this methodology for the standard connection can be defined as:

$$E(x) = \frac{V}{d}\frac{x}{w} \quad (20)$$

Therefore the electrostatic energy stored can be calculated as:

$$W_\varepsilon = \frac{1}{2}\int_{Vol} D.E^2(x)dv = \frac{1}{2}\varepsilon l d\frac{w}{d^2}\frac{V^2}{3} = \frac{1}{2}\frac{C_{ll}}{3}V^2 = \frac{1}{2}C_{eq}V^2 \quad (21)$$

ε: The equivalent dielectric constant of the media interposed between the layers

l: The average turns length

w: The width of the winding window

For the fly back connection configuration we have:

$$E(x) = \frac{V}{2d} \quad (22)$$

$$W_\varepsilon = \frac{1}{2}\int_{Vol} D.E^2(x)dv = \frac{1}{2}\frac{C_{ll}}{4}V^2 = \frac{1}{2}C_{eq}V^2 \quad (23)$$

As it is shown in above equations, if the layers have fly back connection they have lower equivalent capacitance comparing to the standard connection, this is because of the different potential distribution corresponding to the two configurations.

2.4.2 Two layer generalized capacitance model

Figure 8 shows equivalent circuit of two arbitrary layers of a winding. This figure gives us a good imagination for determination of the existence capacitances which are going to be determined for different magnetic components in following chapters. The authors of [3, 16, 23] didn't take into consideration the turn-to-turn capacitance of the turns in the same winding and the following given equations of these six capacitances are based on the static capacitances and electrostatic energy stored between the layers, however in the following chapters all of the turn-to-turn capacitances are taken into accounts for determining the equivalent self-capacitance.

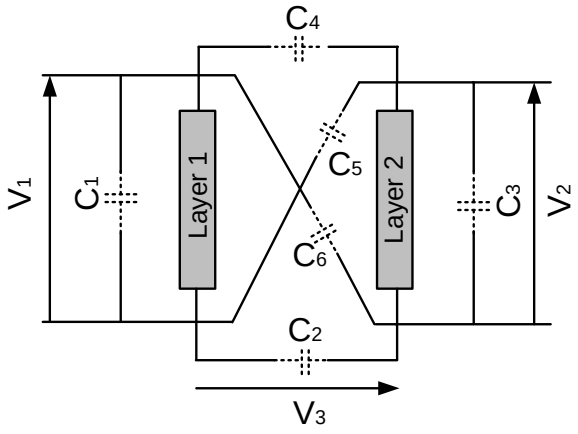

Figure 8: Lumped capacitor network of two arbitrary winding/layer

The equations for the energy storage between the two layers and the six capacitors , shown in Figure 8, [3] are:

$$W_{E,LL} = \frac{C_0}{6}((V_2 - V_1)^2 + 3V_3(V_2 - V_1) + 3V_3^2) \quad (24)$$

$$W_{E,6C} = \frac{1}{2}(C_1V_1^2 + C_2V_2^2 + C_3V_3^2 + C_1(V_2 + V_3 - V_1)^2 + C_5(V_2 + V_3)^2 + C_1(V_3 - V_1)^2 \quad (25)$$

By equation the above two equations and comparing the coefficient of voltages we can determine the value of these six capacitances base on static winding capacitances as following:

$$W_{E,LL} = W_{E,6C}$$

$$C_1 = C_2 = -\frac{C_0}{6}, C_3 = C_4 = \frac{C_0}{3}, C_5 = C_6 = \frac{C_0}{6} \tag{26}$$

3. APPLICATION TO SINGLE WINDING INDUCTORS

3.1 Problem formulation

One of the most critical components in power electronic systems is the high frequency magnetics such as inductors. In high-frequency inductors increasing the operating frequency, the skin and proximity effects cause the winding parasitic resistance to upsurge, and the parasitic capacitance cannot be ignored either. Stray capacitance determines the performance and upper frequency limit of an inductor. The turn-to-turn capacitance and turn-to-core capacitance which are heavily geometry-dependent make an inductor more like a capacitor at high frequencies [42]. It has become widely conscious that parasitic capacitances in high frequency magnetic components, such as single winding inductors, have substantial effects on the performance of the components as well as the entire power electronic systems that contain these magnetic components [35].

These effects are very imperative in high frequency converters, and in topologies which intend to integrate the parasitic effects in the converter topologies. Accepting that the values of the parasitic capacitance in high-frequency inductors can become conclusive in the efficiency of a converter, it would be crucial to accurately predict the response of inductors in high frequency switching mode power supply converters [30].

Photovoltaic inverter is a good example to demonstrate the importance of determining parasitic capacitance of magnetic components. The power electronic inverter is an essential element of the photovoltaic systems as it converts the native

direct-current (DC) from the photovoltaic cells into grid-compatible alternating current (AC), performs maximum power point tracking, and includes safety control and circuitry. Therefore performance, efficiency, and manufacturability are vitally important in the design, cost, and operation of the PV systems. Magnetic components such as inductors and transformers play a significant role in the efficiency and size/weight of inverter. They are also amongst the most difficult components to design, often requiring numerous design interactions and testing. Accurate prediction and design of winding parasitic parameters of high frequency inductors in PV inverters is fundamental to improve performance, lower cost, and speed time to market.

Figure 9 shows different PV inverter topologies including the parasitic capacitances of magnetic components, as it is shown in these topologies, at high frequency, the self-capacitance provides a shunt path around the inductance for the current, thus circumventing the intended filtering operation and as a result the efficiency decreases and maximum energy harvest will not be achieved.

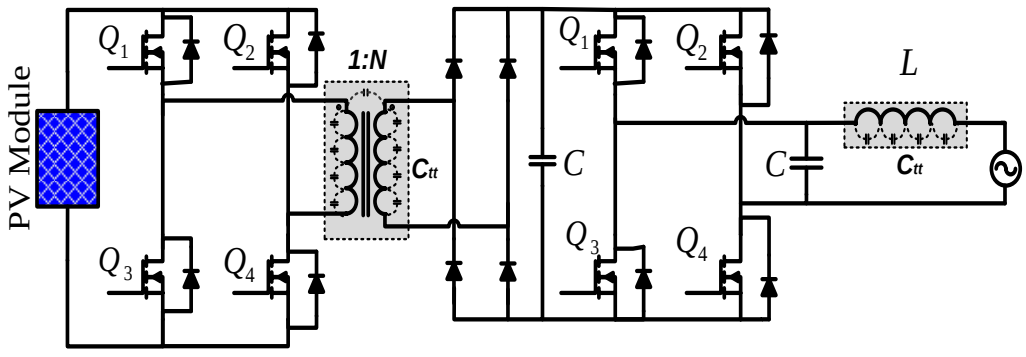

Figure 9: PV inverter topologies including the parasitic parameters of magnetic components

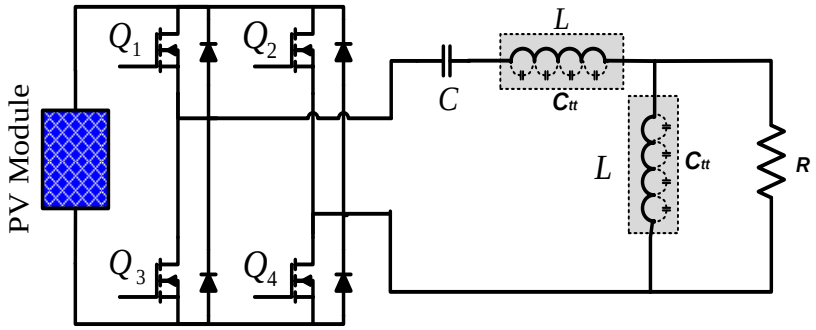

Figure 9: Continued.

3.2 Analytical model and empirical results

3.2.1 Equivalent self-capacitance of a single-layer coil

By using the turn-to-turn capacitance which is determined from previous chapter equation (15), we can find the equivalent self-capacitance of a single-layer coil consisting of n turns wound on a conductive core. Figure 10 shows the lumped capacitor network which is required to be solved in order to find the equivalent self-capacitance.

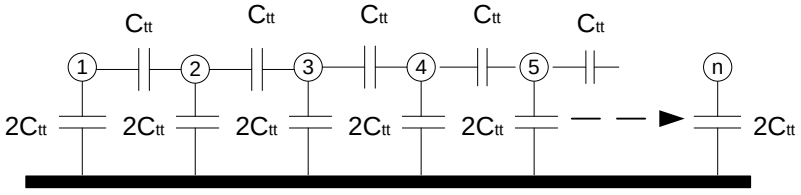

Figure 10: Lumped capacitor network for a single-layer coil with a conductive core

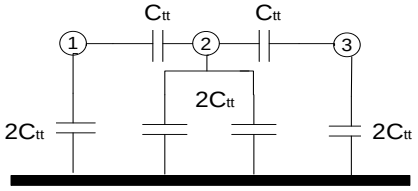

Figure 11: Capacitance for odd number of turns (n=3)

For coils consisting of an even number of turns we first consider the two turns in middle of the coil window. For these turns, *n=2*, where it consists two capacitance between turns 1 and 2, C_{12}, parallel with series combination of the turn to core capacitance C_{1c} and C_{2c}. Since $C_{1c} = C_{2c} = 2C_{tt}$ and therefore the equivalent capacitance of the two turns is given by $C_s = C_{tt} + \frac{2C_{tt}}{2} = 2C_{tt}$ [6]. In the case of an odd number of turns, we first consider the three turns in the middle of the winding, the equivalent capacitance related to *n=3* can be calculated by dividing C_{2c} into two halves, the result is $\frac{C_{tt}}{2} + \frac{C_{tc}}{2} = \frac{C_{tt}}{2} + \frac{2C_{tt}}{2} = \frac{3C_{tt}}{2}$, in order to determine for higher number of turns we can add one more capacitance at each side of the two or three turn coils. Therefore the equivalent self-capacitance can be calculated for *n=4* and *n=5* as following:

$$C_s(4) = \frac{C_{tt}C_s(2)}{2C_s(2)+C_{tt}} + C_{tt} = \frac{7}{5} \times C_{tt} \tag{27}$$

$$C_s(5) = \frac{C_{tt}C_s(3)}{2C_s(3)+C_{tt}} + C_{tt} = \frac{11}{8} \times C_{tt} \tag{28}$$

By increasing the number of turns, we can calculate the equivalent capacitance of coils consisting of any number of turns as following:

$$C_s(n) = \frac{C_{tt}}{2+C_{tt}/C_s(n-2)} + C_{tt} \tag{29}$$

Where $C_s(n-2)$ is the stray capacitance of the coil consisting $(n-2)$ turns, we can see that by increasing the number of turns $(n \geq 10)$, the above equation (29) converges rapidly to well-known equation [6, 7]:

$$C_s \cong 1.366C_{tt}, \quad for\ n \geq 10 \tag{30}$$

By using the above method we can increase the number of layers, for two layer coil the overall self-capacitance with n turns very rapidly converge to well-known equation [6, 7]:

$$C_s \cong 1.83C_{tt} \quad for\ n \geq 10 \tag{31}$$

As it is shown in above equation, two layer coils are affected by higher self-capacitance at high frequency operation. For the three layer coil the overall self-capacitance very rapidly converges to [6, 7]:

$$C_s \cong 0.5733C_{tt} \quad for\ n \geq 10 \tag{32}$$

As it can be seen from above equations the overall self-capacitance of three layer coils is lower than the two and single layer coils with the same geometrical characteristics, but by increasing the number of layers the proximity effect increases. Currents flow in opposite directions in the same conductor of a multiple-layer winding, except for the first layer. Therefore, the amplitudes and rms values of eddy currents caused by magnetic fields in adjacent layers due to the proximity effects upsurge significantly as the number of layers increases [6, 7, 9, 10].

Proximity effect in inductors and transformers increases dramatically with frequency due to eddy current effects, however at low frequencies the current density is uniform and the proximity and skin effects can be neglected. Therefore for design and optimization of high frequency inductors, it is necessarily to accurately predict these winding losses, and base on the accurately determined turn-to-turn capacitance calculate the overall self-capacitance.

3.3 JMAG simulation results

The first step for doing any analysis in JMAG or in any other FEA tool such as Maxwell is to build the geometry model of the case study, in this study an “E core transformer” where the both of the winding placed on center post has been tested. So firstly I built the geometry of transformer in geometry editor of the JMAG, Figure 13 shows the geometry of the model when the mesh has been generated already. In this model the coil has two layers where each layer has 30 turns and 24 AWG winding wires have been used. In order to generate the mesh the first step is to select the analysis that we want to do, since in here we want to calculate the self-capacitance of the coils we should do the “electrostatic analysis” which is available in the “JMAG designer 10.5”, after that we need to apply the material to all of the parts.

It is well known that in any finite element modeling a finer mesh usually results in a more precise solution, but as a mesh is made finer the solution time increases rapidly, therefore in here we firstly can generate the mesh using auto mesh function which automatically auto tune the mesh size to best fit the model. After the mesh has been generated successfully then we can start the electrostatic analysis. In order to calculate the equivalent self-capacitance of the coil, firstly we need to calculate the turn-to-turn capacitance of two adjacent turns in middle of the winding window.

There are several conditions needs to apply to the model after we set the material of the coil and the core which will be discussed in details in this section. In this case study a ferrite “3C90” EE core is used with the dimensions shown in Table 1 and the core represented in Figure 12.

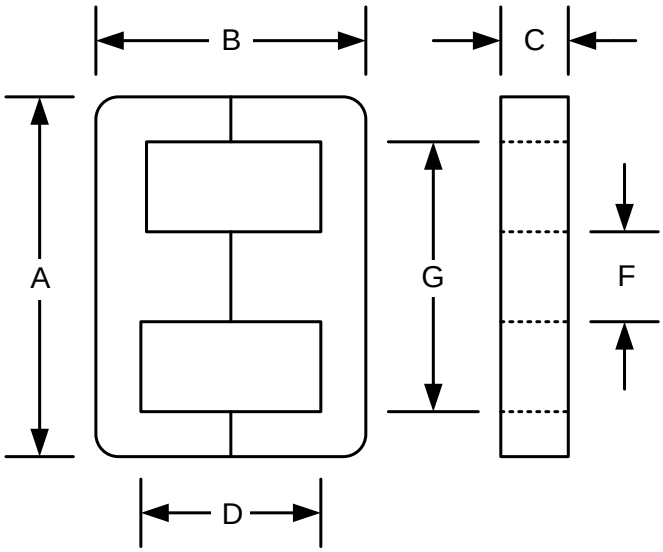

Figure 12: Used EE core with key dimensions

Table 1: Dimentions of used EE core in (mm)

A	46.9± 0.8 mm
B	39.2±0.4 mm
C	15.6±0.25 mm
D	24.2 mm
G	32.4±0.65 mm
F	15.6±0.25 mm

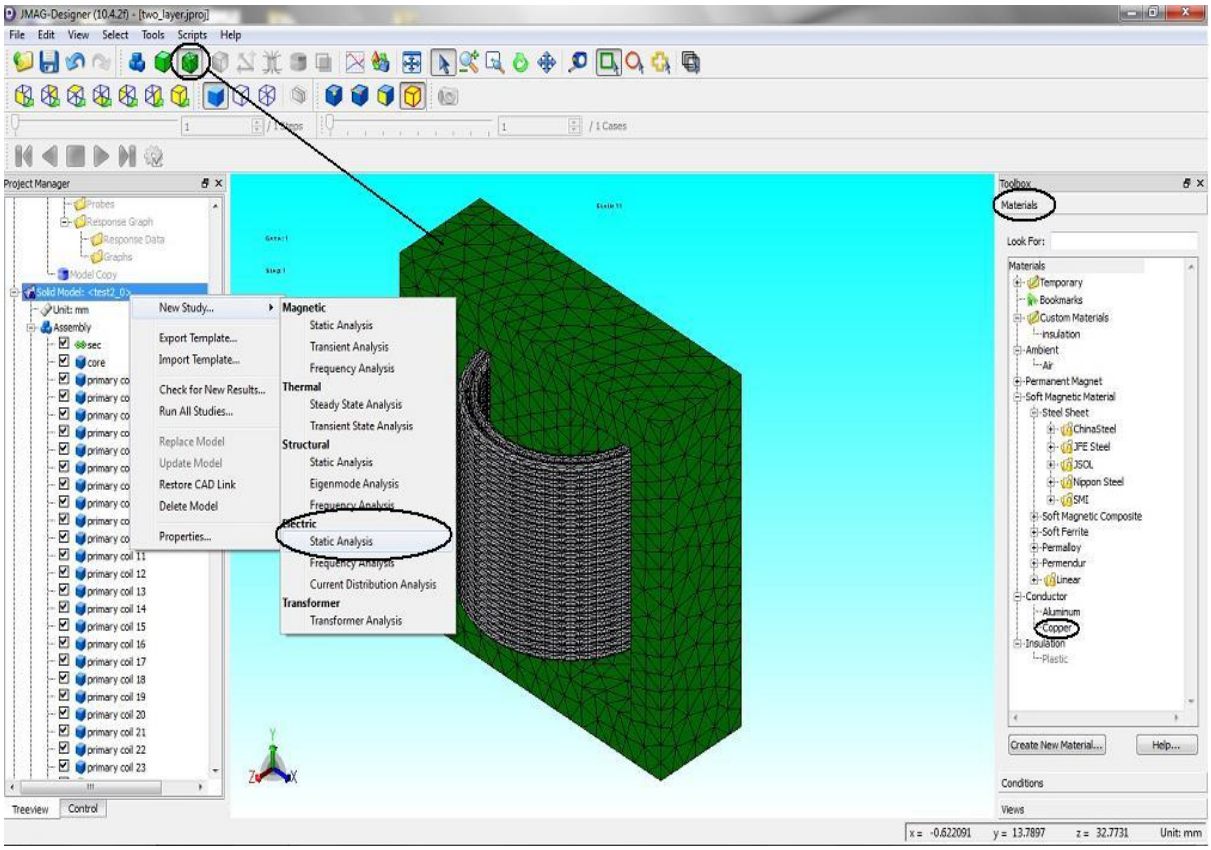

Figure 13: Mesh view of the 3D EE core transformer in JMAG environment

The first step is to calculate the surface charge of these two adjacent conductors, in order to do that we need to apply “Surface Charge” condition to the two neighboring conductors as shown in Figure 14. The next step is to apply the “Electric Potential Boundary” to these turns, this condition specify the electrical potential on specific objects. After that we need to apply the “Symmetry Boundary” condition to the surface of the core where the electric flux flow perpendicular to that surface as it is shown in Figure 15. Finally we should run the electrostatic analysis; this will give us the charge on the surface of these two layers, and by since we have the voltage of them from “Electric

Potential Boundary", assigned to be *1V*, it is possible to calculate the turn-to-turn capacitance of these two contiguous turns in middle of winding window as following:

$$C_{tt} = \frac{Q}{V} = \frac{\oint_S \epsilon E.ds}{-\int_{P_1}^{P_2} E.dl} = \frac{2.87\times10^{-11}}{1} = 28.7\ PF \tag{33}$$

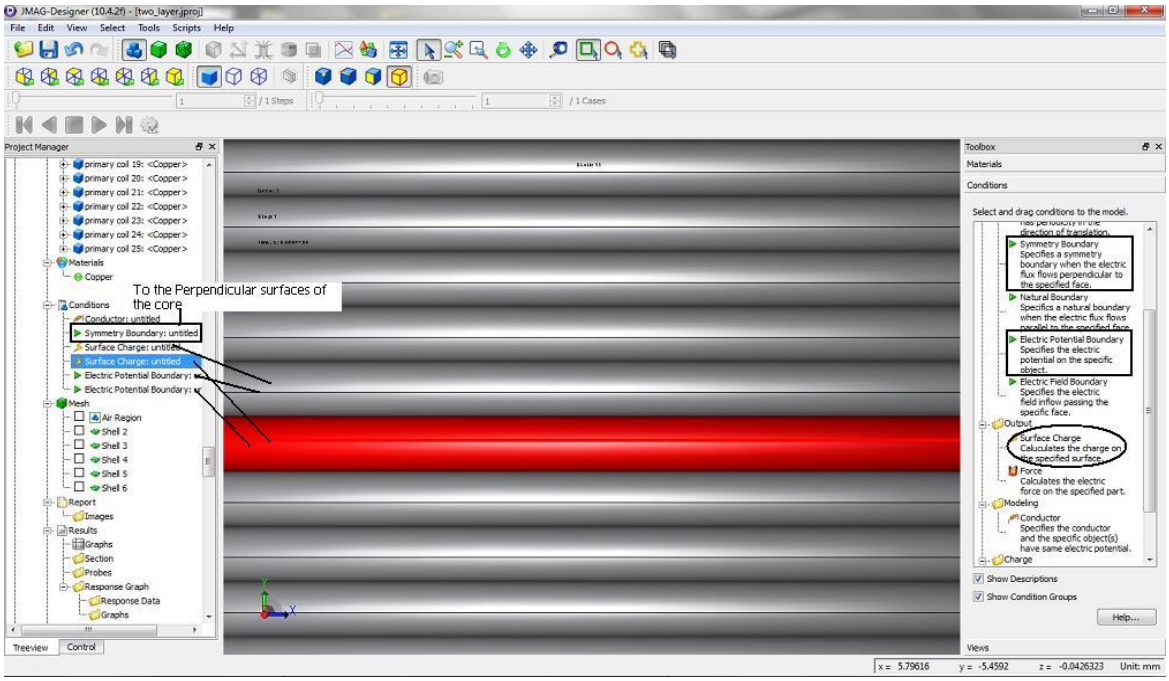

Figure 14: Applying conditions to determine the surface charge

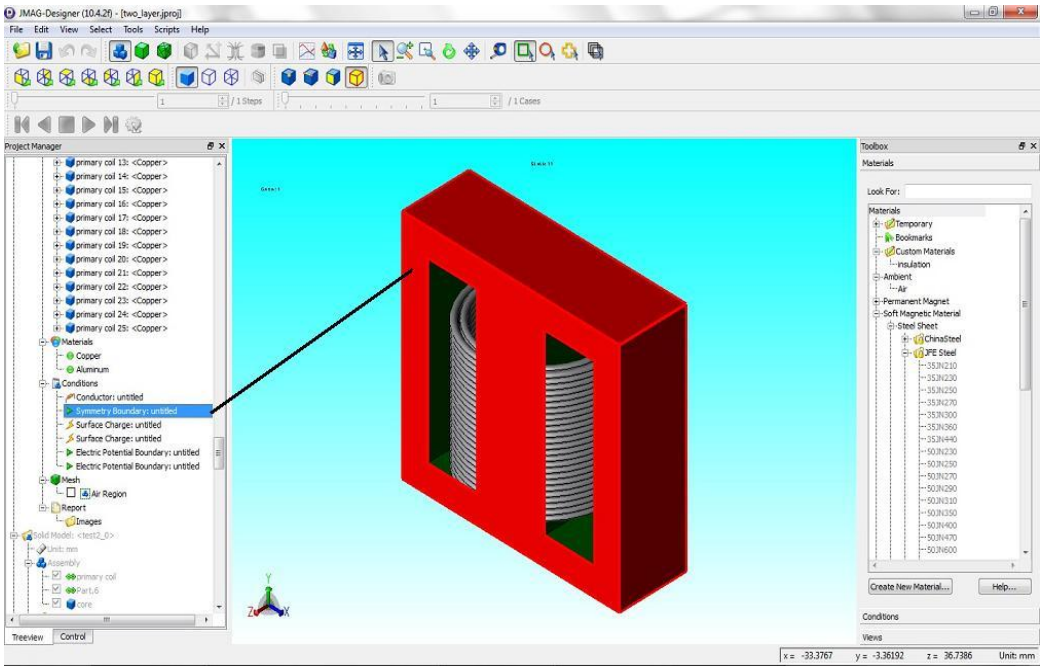

Figure 15: Applying the symmetry boundary condition to the core

The electrostatic analysis of the used FEA tool, JMAG can be used to view the electric field vector plot of the model as it is shown in Figure 17.

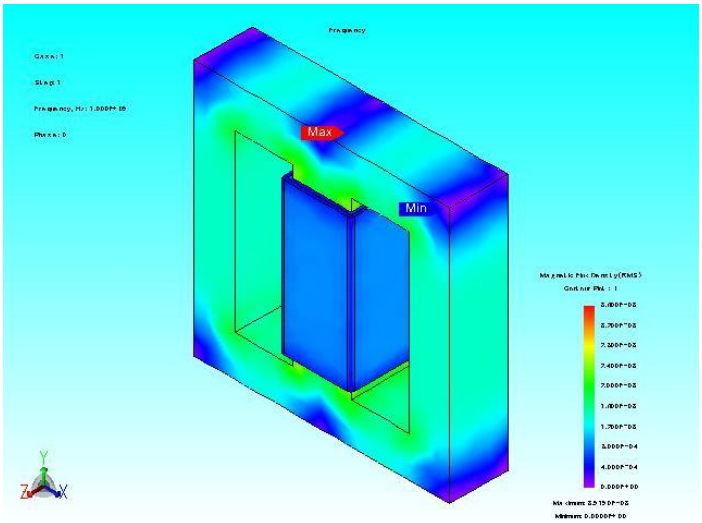

Figure 16: Magnetic flux density of the model

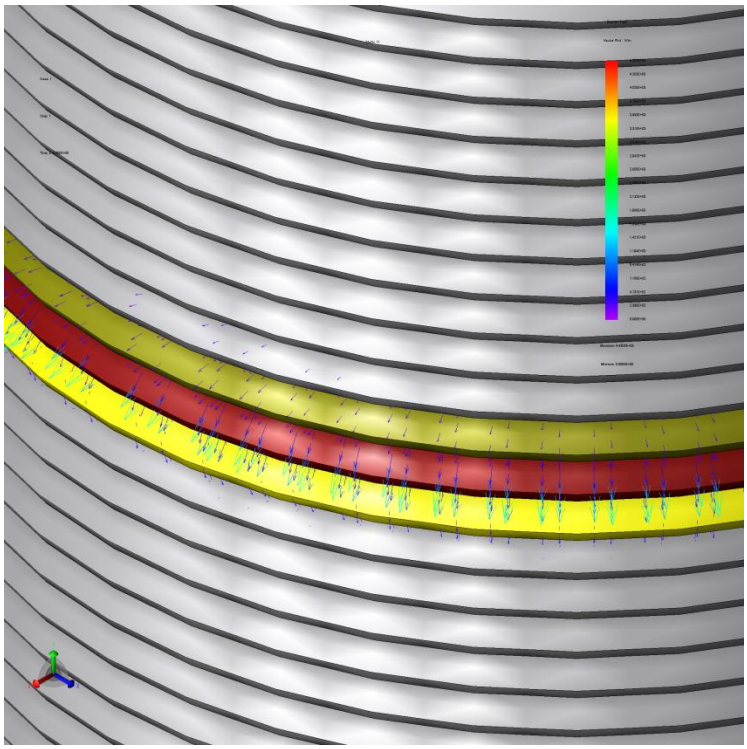

Figure 17: Electric field vector plot of the turns in middle of winding window

3.4 Prototype results

Table 2 shows the summary of simulation, experimental, and empirical formula results, as it is shown they very close to each other and that confirms the methodology used for determining the self-capacitance by the means of FEA tool. The simulation and experimental results are shown good agreement with error of approximately 1.47%.

Table 2: Summary of the simulation, experimental, and emprical formula results

Test Condition	JMAG Simulation	Experimental Results	Empirical Formula
Two Layer Winding with 30 turns on each layer	**52.521 PF**	**51.96 PF**	**49.44**

Figure 18 shows the experimental setup of that model for self-capacitance measurement using RCL meter.

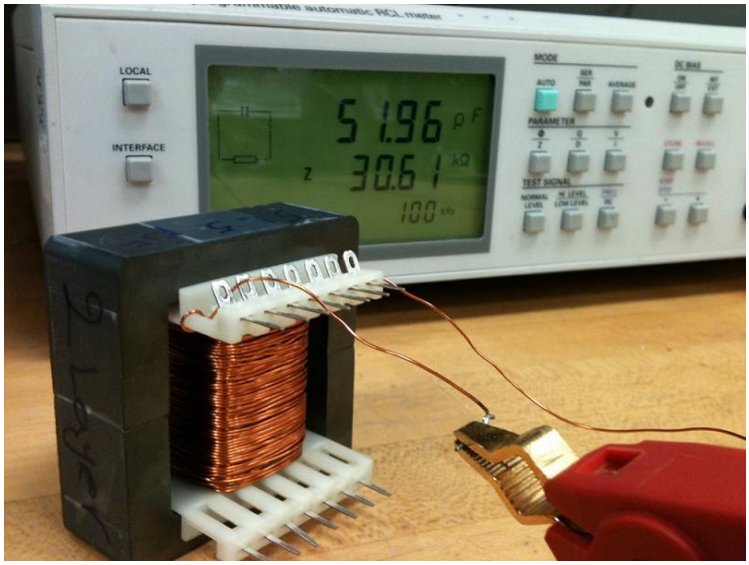

Figure 18: Experimental setup for self-capacitance measurement

4. APPLICATION TO COUPLED INDUCTOR FILTERS*

4.1 Problem formulation

Understanding and predicting parasitic winding capacitance in coupled inductor filters is essential to improve the high-frequency filtering performance. At high frequency, the behavior of coupled inductor filter differs from the low frequency and can be dominated by the parasitic inter- and intra-winding capacitances. This chapter presents a finite element technique to analyze the high-frequency behavior of the coupled inductor filter in a buck converter. Comparison of the FEA results using JMAG with experimental and empirical formula results show good agreement, supporting the method as a model-based design tool with the potential to significantly reduce the design-prototype-test cycle commonly needed with sophisticated magnetic designs.

A coupled inductor filter offers numerous filtering advantages including "notch mode" behavior that makes it advantageous for use in switch mode power supplies [43]. However, the parasitic capacitance which arises from capacitance between adjacent windings turns can reduce the impedance of the coupled-inductors at high-frequency, therefore diminishing the effectiveness for high frequency filtering [17, 21, 44]. Figure 19 shows the common equivalent circuit of a single winding structure where L is the inductance of the winding, R is the resistance of the winding, and C_s is the equivalent

self-capacitance of the winding.

At low frequency, stray self-capacitance, core losses, skin and proximity effects can be neglected. However, at high frequency, such as harmonics of the switching frequency, the equivalent circuit model fails to accurately capture the true performance.

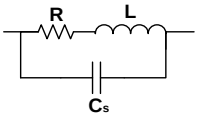

Figure 19: Equivalent electrical circuit for the winding of inductor

The aim of this chapter is the accurate calculation of the parasitic capacitance of a high frequency coupled inductor filters for use as the input filter of a dc/dc "buck converter" using the finite element analysis (FEA) tool JMAG. Unlike analytical or empirical techniques, finite element analysis has the ability to take into consideration the physical properties of the materials as well as the construction of the winding structure. This chapter also presents the derivation of empirical formula of parasitic capacitance of inductors in order to compare the simulation results of FEA tool with the empirical formula and experimental results.

The input filter for a buck converter is an example of one application for the coupled inductor filter. Figure 20 shows the filter structure as well as the parasitic self-capacitance for each of the two coupled inductors in the filter. At high frequency, the self-capacitance provides a shunt path around the inductance for the current, thus circumventing the intended filtering operation. Additionally, the presence of this capacitance may complicate experimentally measuring the coupling coefficient k at high-frequencies. Frequently these parasitic capacitances are not included in circuit

simulations, but are easily observed when a network analyzer is used to obtain the bode plot of a prototype of coupled inductor filters [45].

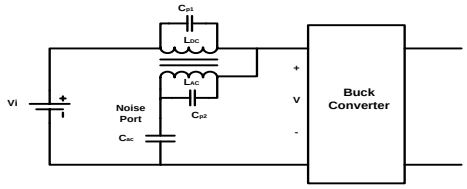

Figure 20: Coupled inductor filter including parasitic capacitances.

Since the coupling coefficient and parasitic capacitances are highly dependent on the method of construction, a model-based design tool is needed to reduce the design-prototype-test cycle. Calculation of the coupling coefficient, which is highly dependent on the physical properties of the model, can be predicted accurately base on this FEA tool methodology. Knowing the coupling coefficient accurately enables the designer to ensure that the coupled inductor always operates in the notch mode for extra attenuation at the notch frequency [45]. There are several parasitic capacitance cancelation techniques for coupled inductor filters which are presented in [46, 47]; the accurate prediction of these capacitances will increase the efficiency of parasitic capacitance cancelation and as a result more perfect inductor filters.

4.2 Principle of operation

4.2.1 Modes of operation

The coupled inductor in Figure 21 can be represented by magnetizing and leakage inductances shown in Figure 22. The inductor *M* is the mutual inductance of the two coils and is related to the coil inductances as:

$$M = k\sqrt{L_{ac}L_{dc}} \tag{34}$$

The coupling coefficient is $0 < k < 1$, the coupling coefficient describes the magnetic circuit and is a function of numerous factors, including magnetic flux path geometry. By using the proposed methodology in JMAG for determination of *k*, a higher efficient filter can be achieved because changes in wire spacing or changes in winding technique can cause variations in *k* and the proposed methodology take into consideration all of these physical effects. This will be important because the operating regime of the coupled inductor is sensitive to *k* [43].

$$G(s) = \frac{V_q}{V_n} = \frac{1+s^2 C_{ac} L_{ac}\left(1-k\sqrt{\frac{L_{dc}}{L_{ac}}}\right)}{1+s^2 C_{ac} L_{ac}} \tag{35}$$

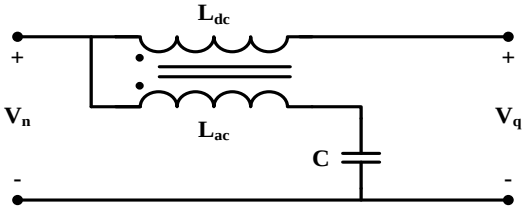

Figure 21: Coupled inductor filter

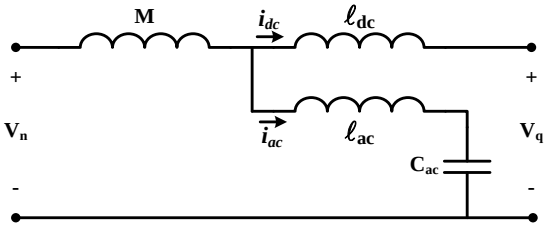

Figure 22: Equivalent uncoupled inductor filter

The frequency of the zero in this transfer function depends on the coupling coefficient *k*; therefore the interesting mode of operation occurs at a unique value called the null condition:

$$k_{null} = \sqrt{\frac{L_{ac}}{L_{dc}}} \tag{36}$$

At null condition, the coupled inductor filter will operate equivalently to a second order filter, as shown in Figure 23. Thus the null condition is a boundary value for the formation of a notch shown in Figure 23. For coupling coefficient values less than k_{null}, the transfer function zero frequency is greater than the pole frequency and a notch appears. At the notch frequency additional attenuation can be achieved, this is one of the most significant advantages of coupled inductor filter over the conventional filters [43, 45]. If the coupling coefficient be greater than k_{null}, there is no notch and high frequency attenuation is worse compared to a simple second order filter.

The frequency of the notch can be determined by taking into consideration the numerator of (35) L_{ac} and C_{ac} form a series resonant circuit, and reducing the impedance of that branch to zero for the frequency given by:

$$\omega_{notch} = \frac{1}{\sqrt{CL_{ac}\left(1-k\sqrt{\frac{L_{dc}}{L_{ac}}}\right)}} \tag{37}$$

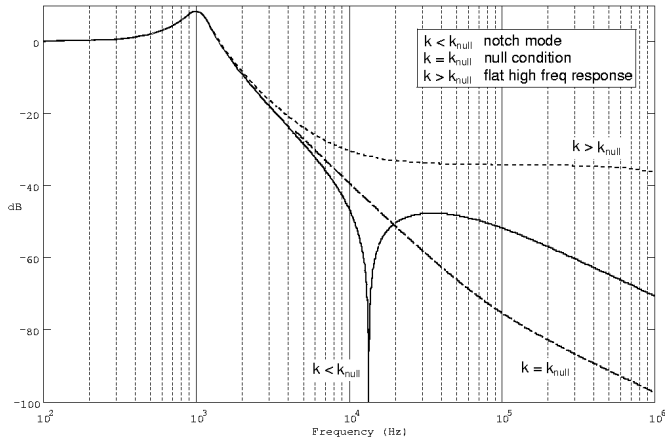

Figure 23: Modes of operation

4.2.2 Analytical model

The coupled inductor is redrawn here as Figure 24 with existing inter-winding and intra-winding capacitances. It is convenient to mark the windings as “dc” and “ac” where the dc winding carries the heavy direct current, while the ac winding carries only a small ac ripple current. As mentioned in previous section, at high-frequency the self-capacitances appear in series and provide a bypass current path around the magnetically-coupled windings [43].

Figure 25 shows the geometry model of the couple inductor including the parasitic capacitances of the case study which is going to be reviewed in this chapter. For more clarification the lumped network capacitor of the ac winding is drawn. The magnetic coupling between the ac and dc windings is specified to attain the anticipated filter performance. Inter-winding capacitance creates an electrical coupling in parallel with the magnetic coupling and consequently deserves special design consideration to guarantee that the desired notch is not undesirably affected [43]. Therefore it is necessary to determine this coupling coefficient. In this section an analytical magnetic model of the coupled inductor will be discussed.

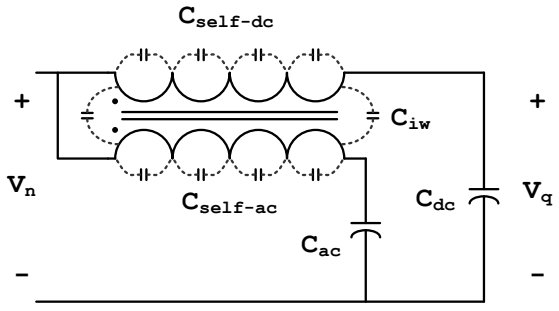

Figure 24: Parasitic capacitances of typical coupled inductors

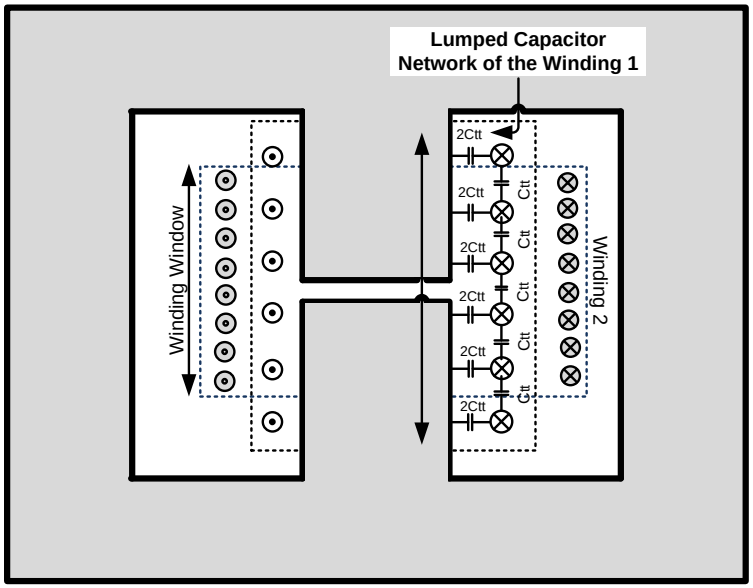

Figure 25: Case study for determination of self-capacitance of odd number of turns

Since a two winding inductor is going to be modeled and analyzed, the analytical model going to be generalized for a *N* winding magnetic components where all of the windings are placed around a common core, Figure 26. Fundamental theory of coupled inductor says that the average flux per turn of winding *k* is given by [2]:

$$\emptyset_k(t) = \emptyset_c(t) + \sum_{m=1}^{N} \emptyset_{km}(t) \tag{38}$$

Which is the summation of the core flux, $\emptyset_c(t)$, and the flux induced in winding *k* by winding *m*. The voltage of winding *k* can be represented by:

$$V_k(t) = N_k \frac{d\emptyset_k(t)}{dt} \tag{39}$$

By taking into consideration the linear relationship between the fluxes and currents, and using the above two equations, the voltage of winding *k* can be shown as:

$$N_K \emptyset_{km}(t) = L_{km} i_m(t)$$

$$V_k(t) = N_k \frac{d\emptyset_c(t)}{dt} + \sum_{m=1}^{N} L_{km} \frac{di_m(t)}{dt} \quad (40)$$

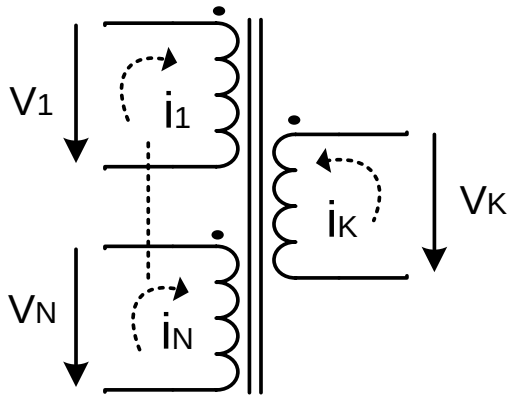

Figure 26: *N*-winding magnetic component on a common core

The superposition theorem can be used for deriving the parameters values of the model [2]. Usually a linear system is required for applying the superposition principle, but the only non-linear component in here is the core. It is not the aim of this study to take into consideration the core model and as a result the non-linearity behavior and the saturation of the core are not taken into consideration, because if the non-linearity appears the field distribution in the magnetic components changes as well as the parasitic, the goal of this thesis is the modeling of the winding structure. So a constant value of permeability is used in the FEA tool to be able to apply the superposition theorem. This doesn't represents a serious limitation for the magnetic components such as coupled inductors and multi-winding transformers for use in switch mode power supplies because they are almost always designed to work in the linear region.

The main idea for determination of the model parameters are based on the energy equations where the field can be determined by a FEA tool. The flux based methodology is not always applicable for several reasons:

- The self and mutual fluxes are not easy to calculate
- As the geometry becomes more complex, the calculation of the flux will be more problematic

By applying current $i_k(t) = I_0 \sin(\omega t)$ into winding k, a magnetic field $H_k(x, y, z, t)$, H_k is a vector which components in x, y, and z axes are sinusoids of pulsating frequency ω, appears in every point of the magnetic component. Phasors can be defined for electromagnetic magnitudes, $\overrightarrow{I_{k0}}, \overrightarrow{B_{k0}}$, and $\overrightarrow{H_{k0}}$, since the magnetic components are operating in sinusoidal regime. The total magnetic induction and magnetic field in any point of component by applying superposition can be represented as:

$$\overrightarrow{B_0} = \sum_{k=1}^{N} \overrightarrow{B_{k0}} \ , \ \overrightarrow{H_0} = \sum_{k=1}^{N} \overrightarrow{H_{k0}} \tag{41}$$

The total energy storage in the windings and all space around it depends on two kinds of terms, one depends on the field created by the current of one winding (*i)*, and the other depends on the fields produced by two different windings (*i* and *j)* is given by:

$$W = \frac{1}{4} \iiint_V Re(\overrightarrow{B_0}.\overrightarrow{H_0^*}) dv \tag{42}$$

$$W = \frac{1}{4} \sum_{i=1}^{N} \iiint_V \overrightarrow{B_{i0}}.\overrightarrow{H_{i0}^*} dv + \frac{1}{2} \sum_{i=1}^{N-1} \sum_{j=i+1}^{N} \iiint_V \overrightarrow{B_{i0}}.\overrightarrow{H_{i0}^*} dv \tag{43}$$

Figure 27 shows the equivalent circuit including inductances, the average energy stored in this circuit is given by:

$$W = \frac{1}{4}\sum_{i=1}^{N} L_{ii} I_0^2 + \frac{1}{2}\sum_{i=1}^{N-1}\sum_{j=i+1}^{N} L_{ij} I_0^2 \quad (44)$$

By equation the above both average equation the value of the inductances of the equivalent circuit can be determined as following:

$$L_{ii} = L_{ij} = \frac{1}{I_0^2} \oiiint_V Re\,(\overrightarrow{B_{\iota 0}}.\overrightarrow{H_{\iota 0}^*})dv \quad (45)$$

The core inductance referred to winding *k* when a current is injected into that, L_{mk}, is the volume integration (c+g) occupied by the magnetic core (c) and the core gap (g) which is given by:

$$L_{mk} = \frac{1}{I_0^2} \oiiint_{c+g} Re\,(\overrightarrow{B_{k0}}.\overrightarrow{H_{k0}^*})dv \quad (46)$$

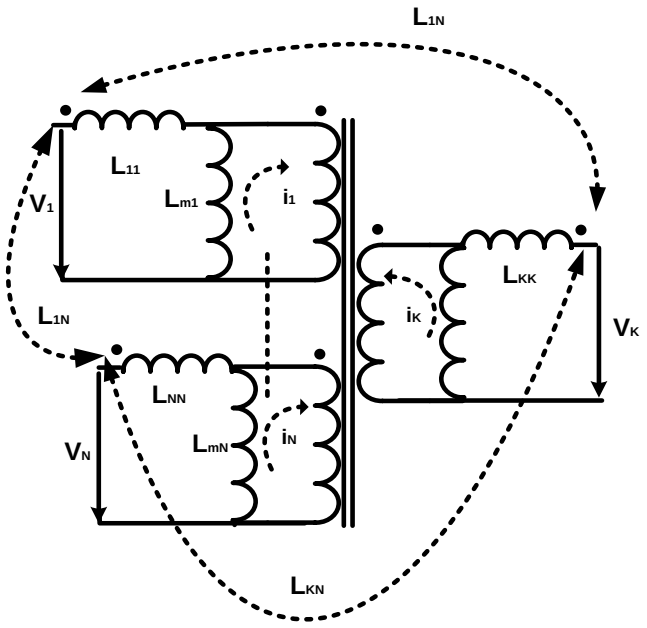

Figure 27: Equivalent circuit of the magnetic effects model

Now by using the determined value of these inductances base on the energy storage, we can determine the coupling coefficient of a coupled inductor as discussed more in details in previous section by following equation:

$$k = \frac{M}{\sqrt{L_{ac}L_{dc}}} \tag{47}$$

4.3 JMAG simulation results

Figure 28 shows briefly the proposed methodology for determination of self-capacitance in JMAG. In order to calculate the equivalent self-capacitance of the coil, firstly we need to calculate the turn-to-turn capacitance of two adjacent turns in middle of the winding window. There are several conditions needs to apply to the model after we set the material of the coil and the core. The first step is to calculate the surface charge of these two adjacent turns, in order to do that we need to apply *"Surface Charge"* condition to the two neighboring turns. The next step is to apply the *"Electric Potential Boundary"* to these turns, this condition specify the electrical potential on specific objects. After that we need to apply the *"Symmetry Boundary"* condition to the surface of the core where the electric flux flow perpendicular to that surface. Therefore by knowing the electric potential boundary of these turns and the surface charge we will be able to determine the turn-to-turn capacitance as it is shown in the following algorithm.

In this study a "3C90" ferrite "EE core", Figure 29, with the dimensions mentioned in Table 3 has been tested where both of the winding placed on the center post. Figure 30 shows the two-winding inductor built in JMAG and its magnetic flux

density distribution vector plot. Table 4 shows summary of the simulation, practical, and empirical results for the case study of 24 AWG windings at 100 kHz.

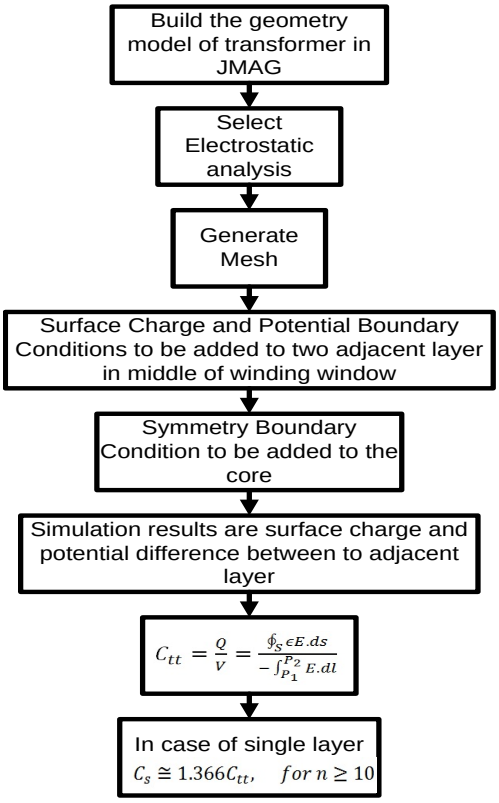

Figure 28: Procedure for determination of self-capacitance using FEA tool

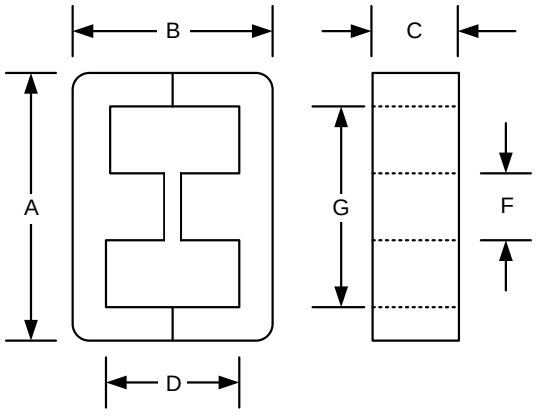

Figure 29: Used EE core key dimensions with air gap

Table 3: Dimensions of the used EE core in (mm)

A	46.9± 0.8 mm
B	39.2±0.4 mm
C	15.6±0.25 mm
D	24.2 mm
G	32.4±0.65 mm
F	15.6±0.25 mm
Total Air Gap	≈ 0.86 mm

Because of the key role of the coupling coefficient in the notch-mode of the coupled inductor filtering *k* has been calculated by means of FEA tool for the case study shown in Figure 30.

$$k = \frac{M}{\sqrt{L_{AC}L_{DC}}} = \frac{4.332\times10^{-5}}{\sqrt{6.81\times10^{-5}\times3.014\times10^{-5}}} = 0.956 \quad (48)$$

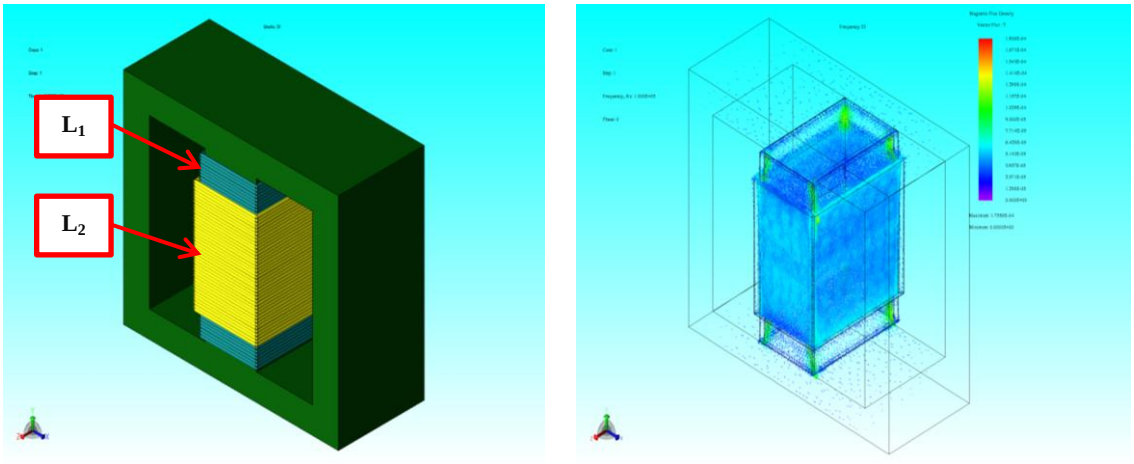

(a) **(b)**

Figure 30: a) two-winding inductor built in JMAG b) magnetic flux density distribution vector plot

4.4 Prototype results

Table 1 shows the summary of experimental, simulation, empirical formulas results. As it is represented in the experimental prototype shown in Figure 32, the simulation and experimental results shows acceptable agreement with error of approximately 2.5%.

Table 4: Summary of simulation results and experimental results with L1 of 60 turns and L2 of 40 turns

	C_{S1} (Double layer, each layer 50 turns) of L_1	C_{S1} (Single layer 60 turns) of L_1
Simulation	**60.04 PF**	**41.34 PF**
Experimental	**58.55 PF**	**39.61 PF**
Empirical formula	**54.16 PF**	**44.11 PF**
% Error of Simulation Vs. Experimental	**2.54%**	**4.36%**
% Error of Experimental Vs. Empirical	**7.49%**	**11.36%**

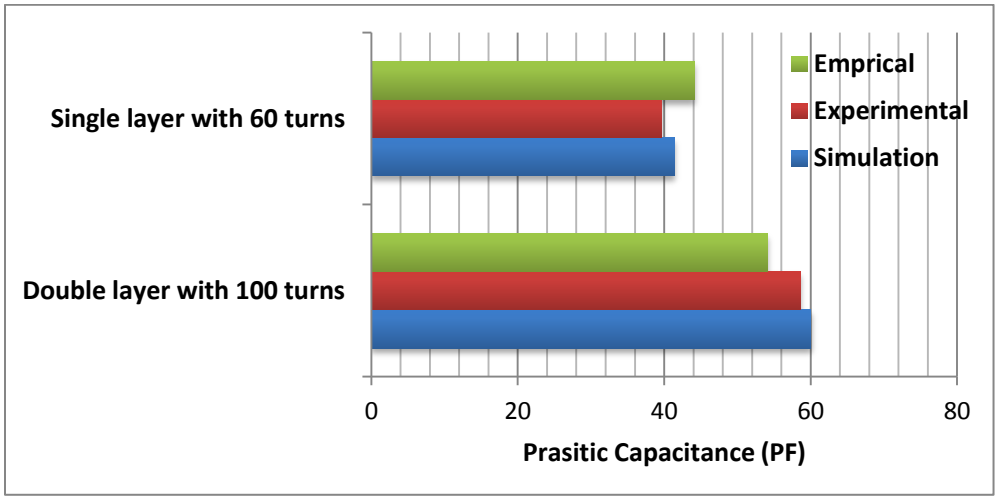

Figure 31: Comparison of simulation, experimental, and empirical results for coupled inductor

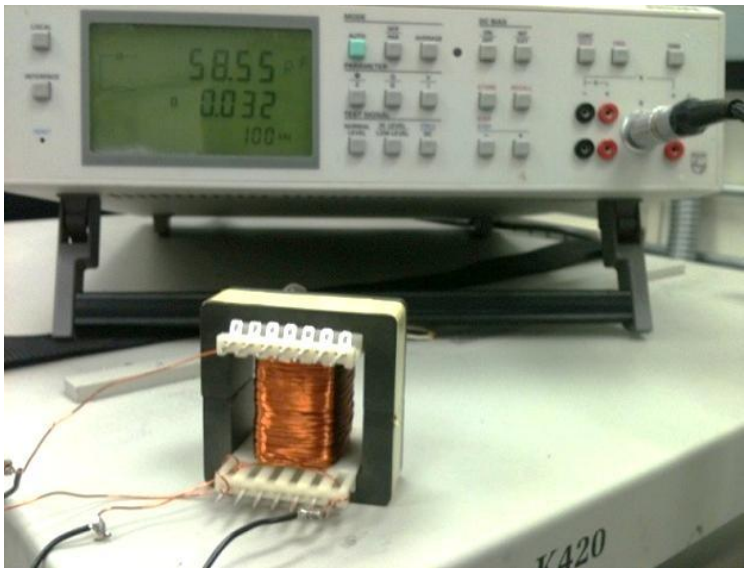

Figure 32: Experimental setup for double layer, each layer 50 turns

As it is shown in Table 4, the empirical formula is not as accurate as in the single winding structures because these empirical formulas are derived base on simple single winding structures, therefore the use of the proposed methodology is more significant in this application.

5. APPLICATION TO MULTI-WINDING TRANSFORMERS

5.1 Problem formulation

For several basic magnetic devices such as the single winding inductors, the parasitic components equations can be derived, but deriving these equations will be much more difficult and almost impossible for more complicated geometries such as multi-winding transformers. Several techniques such as interleaving of layers of the windings can be used to lower the winding capacitances as well as other parasitic parameters [36, 48], but these techniques make the geometry of the model more complicate. Parasitic capacitances are difficult to model because of the non-uniform electric fields involved and the fact that the fields are a function of the configuration in which the transformer is used. In addition engineers need to be build and test to get the right geometry, Figure 33 shows different multi-winding transformers which are usually built to get the right geometry with lowest parasitic capacitances.

Figure 34 shows the cycle which is needed by magnetic designers and power electronics engineers for testing each prototype, this cycle is usually a week or more. Therefore it is necessarily to have a design-oriented framework to determine the inter- and intra-winding capacitances of multi-winding transformers. The importance of the proposed methodology can be seen here more significantly than previously discussed applications because the derived empirical formulas in literature [10] is not applicable for complicated geometry of multi-winding transformers such as the case study of this chapter which usually needed for use in switching power supplies, in the other hand it is

almost impossible to derive the analytical equations that describe the behavior of magnetic components.

Figure 33: Several multi-winding transformer usually built to get the right geometry

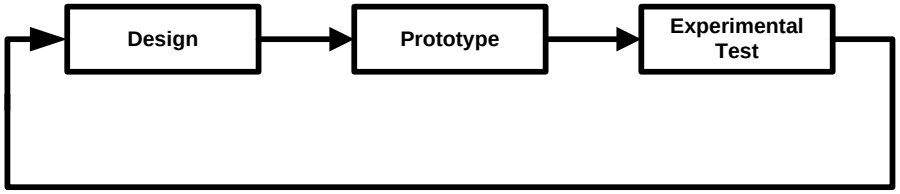

Figure 34: Required cycle for testing each prototype

Capacitive effects of transformers are the least studied ones of the magnetic components in literature [3, 13, 15, 18, 19, 24, 35, 49, 50], these studies are based on simple two winding transformers and most of them showing different methods for deriving analytical equations these two winding transformers. These parasitic

capacitances affect the power supply current and voltage waveforms. Because of existence of high frequency current in multi-winding transformer windings which goes through the low value capacitive impedances of these windings, therefore it is needed to have a methodology for generating a model for high frequency multi-winding transformers by means of a FEA tool. This chapter proposes a FEA methodology for determining parasitic capacitances of multi-winding transformers with more complicated geometries than the earlier discussed applications.

5.2 Analytical model

The superposition usually applied for deriving the analytical models of high frequency transformers. If core saturation is presented the superposition theorem is not applicable for deriving the analytical models, but this is not a serious problem for the transformers using in switching mode power supplies because they work in linear region [1, 24, 51].

The first step for determining the parasitic capacitances is to calculate the energy stored in the electric field, as discussed in earlier chapters. Two main kinds of voltages should be taken into consideration for analysis in a transformer:

- The voltage across the terminals of the windings
- The voltage between ground and a winding terminal

The voltages across the terminals of the windings are the floating voltages which are in all of the windings. There are several limitations imposed to the previously

mentioned voltages for modeling of capacitive effects in the winding of transformers, Figure 35 [2]:

- The voltages of all of the windings are related by turns ratio
- They have also a voltage offset referred to ground

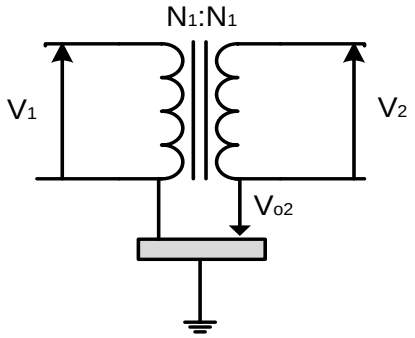

Figure 35: Voltages of a two winding transformers

As represented in Figure 35, winding 1 has a voltage $V_1(t)$ in a N winding transformer, and the $N-1$ voltages across the terminals of the other $N-1$ windings are:

$$V_k(t) = \frac{N_k}{N_1} V_1(t) \tag{49}$$

All of these voltages produce an electric filed $E_1(t)$ in the windings, also the offset voltages $V_{ok}(t)$, produces an electric field $E_{ok}(t)$. Therefore the electric field and the displacement field can be calculated as following:

$$E(t) = E_1(t) + \sum_{k=2}^{N} E_{ok}(t) \tag{50}$$

$$D(t) = \varepsilon E(t) = \varepsilon_0 \varepsilon_r E(t) \tag{51}$$

As a result, the energy stored in the electric field can be determined by [14]:

$$w(t) = \frac{1}{2} \iiint_V D(t).E(t)dv = \frac{1}{2} \iiint_V \varepsilon_0 \varepsilon_r E(t).E(t)dv \tag{52}$$

Then from above three equations we have:

$$w(t) = \frac{1}{2}\iiint_V \varepsilon_0\varepsilon_r E(t).E(t)dv =$$

$$\frac{1}{2}\iiint_V \varepsilon_0\varepsilon_r E_1(t).E_1(t)dv + \sum_{i=1}^{N}\frac{1}{2}\iiint_V \varepsilon_0\varepsilon_r E_{oi}(t).E_{oi}(t)dv +$$

$$\sum_{i=1}^{N}\iiint_V \varepsilon_0\varepsilon_r E_1(t).E_{oi}(t)dv + \sum_{i=1}^{N-1}\sum_{j=i+1}^{N}\iiint_V \varepsilon_0\varepsilon_r E_{oi}(t).E_{oj}(t)dv \quad (53)$$

There are four terms in above energy stored equation which depends on:

- First term depends on the existence of the voltages across the terminals of the windings
- Second term depends on the existence of one offset voltage
- Third term depends on the simultaneous action of two voltages $V_1(t)$ and $V_{oi}(t)$
- The fourth term depends on the simultaneous action of two voltages $V_{oi}(t)$ and $V_{oj}(t)$

For sake of conciseness, capacitances of a three winding transformers going to be modeled in this section, but in the next section a more intricate geometry going to be design and determining its parasitic capacitances by means of FEA tool. Figure 36 shows the inter- and intra-winding capacitances of a three winding transformers which are going to be modeled. Firstly the energy stored by the capacitors can be calculated as following:

$$w(t) = \frac{1}{2}\left[C_1 + \sum_{j=2}^{N} C_{1j}\right]V_1^2(t) + \left[\frac{1}{2}\sum_{i=2}^{N}(C_{oi} + C_{1i}) + \sum_{i=1}^{N-1}\sum_{j=i+1}^{N} C_{oij}\right]V_{oi}^2(t) -$$

$$\sum_{i=1}^{N} C_{1i}V_1(t)V_{oi}(t) - \sum_{i=1}^{N-1}\sum_{j=i+1}^{N} C_{oij}V_{oi}(t)V_{oj}(t) \quad (54)$$

By equating the equations 54 and 53, the parasitic capacitances can be determined as they are shown in Table 5.

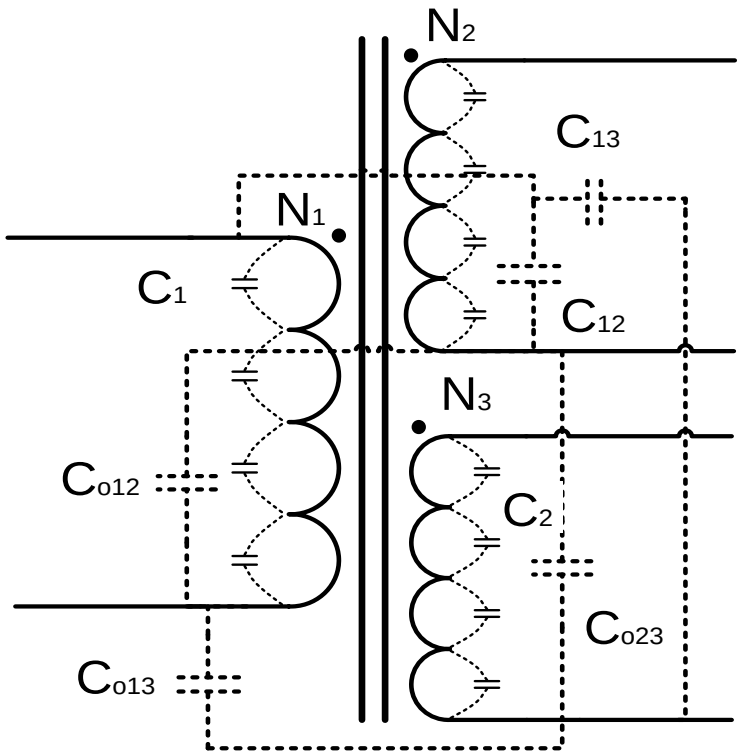

Figure 36: Inter- and intra-winding capacitances of a three winding transformers

Table 5: Parasitic capacitance models of three winding transformers

$C_1 = \frac{1}{U_1^2}\oiiint_V \varepsilon_0\varepsilon_r E_1(t).E_1(t)dv - \sum_{j=2}^{N} C_{1j}$	(55)
$C_{oij} = -\frac{1}{2U_{oi}U_{oj}}\oiiint_V \varepsilon_0\varepsilon_r E_{oi}(t).E_{oj}(t)dv$	(56)
$C_{1i} = -\frac{1}{2U_1U_{oi}}\oiiint_V \varepsilon_0\varepsilon_r E_1(t).E_{oi}(t)dv$	(57)
$C_{1i} + C_{o1i} = \frac{1}{U_{oi}^2}\oiiint_V \varepsilon_0\varepsilon_r E_{oi}(t).E_{oi}(t)dv - \sum_{\substack{j=2 \\ j\neq i}}^{N} C_{oij}$	(58)

5.3 Case study and JMAG simulation results

In this section a multi-winding transformers are going to model and determining the matrix of parasitic capacitances by means of a FEA tool, JMAG. The multi-winding transformer which is modeled including the parasitic capacitances is represented in Figure 37, as it is shown in this figure these types of transformers commonly utilize in PV systems.

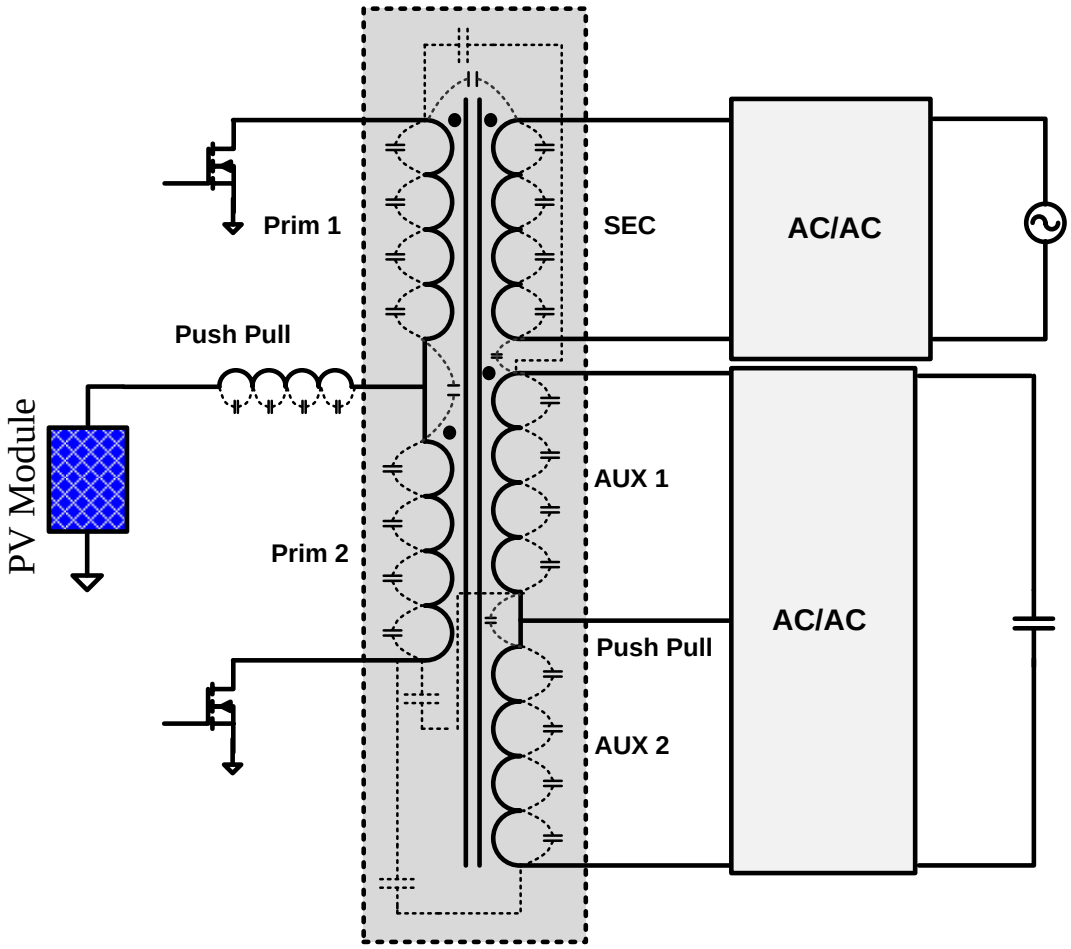

Figure 37: Multi-winding transformer including the parasitic capacitances used in SMPS

Figure 38 shows the physical cross section view of the built multi-winding prototype which is going to modeled in JMAG. The entire transformer specifications are represented in Table 6 and Table 7.

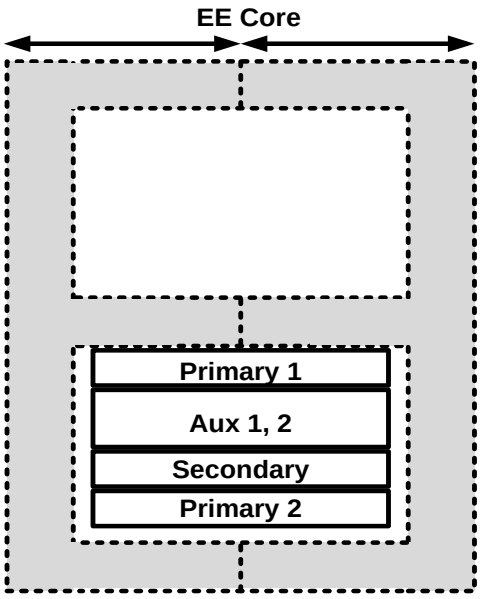

Figure 38: Physical cross section view of the multi-winding transformer

Table 6: Multi-winding transformer specifications

Parameters	Value
Primary winding voltage (V_{pri})	60 V
Secondary winding voltage (V_{sec})	373 V
Auxiliary winding voltage (V_{aux})	350 V
Excitation Frequency	8 kHz
Tot primary RMS winding current	3.33 A
Tot secondary RMS winding current	0.926 A
Tot auxiliary RMS winding current	0.864 A
Pulse Duration	62.5×10^{-6} s

Table 7: Winding specifications

Windings	Number of turns	Thickness (AWG)	Inductance (mH)
Primary winding	24	25 AWG	2.5 mH
Secondary winding	150	25 AWG	98.8 mH
Auxiliary winding	140	26 AWG	86.1 mH

As it is shown in Figure 39, an *EE60/44/16* core is used with the dimensions represented in Table 8.

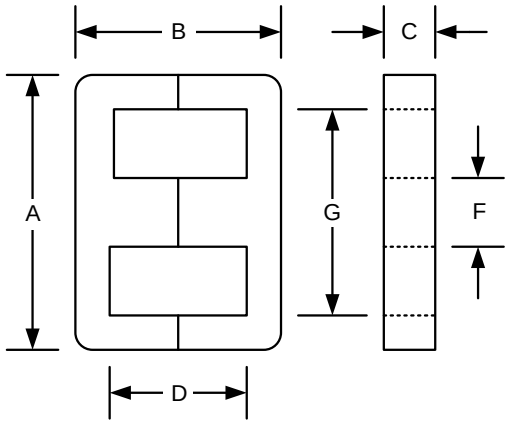

Figure 39: Used EE core with key dimensions

Table 8: Dimentions of used EE core for multiwinding transformer in (mm)

A	60 ± 1.2 mm
B	88 ± 0.6 mm
C	16 ± 0.25 mm
D	68 ± 0.8 mm
G	40 ± 1.8 mm
F	20 ± 0.7 mm

The procedure employed for the coupled inductor application in previous chapter can be utilized for this multi-winding transformer to determine the self-capacitance, Figure 28. The inter-winding capacitance by means of the FEA tool can be determined as:

1) Applying 1 V to a specific winding and 0 V to the other winding
2) Calculating the scalar electric potential *V*
3) Computing the electric field strength and the electric flux density from *V*
4) Determining the capacitance values by computing the energy stored in the field

The analytical parasitic capacitance equations base on the energy stored in the field derived in the previous section and summarized in Table 5.

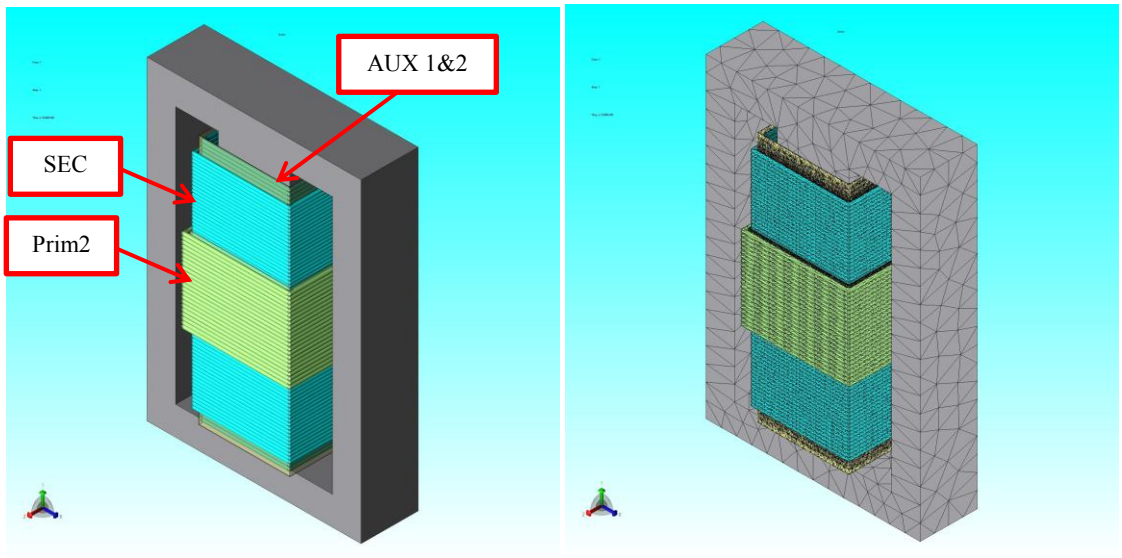

(a) (b)

Figure 40: a) built model in JMAG b) mesh view of the model

Figure 40 shows the model built in JMAG and the mesh view of the model, a more detailed model including the mesh view are shown in Figure 41.

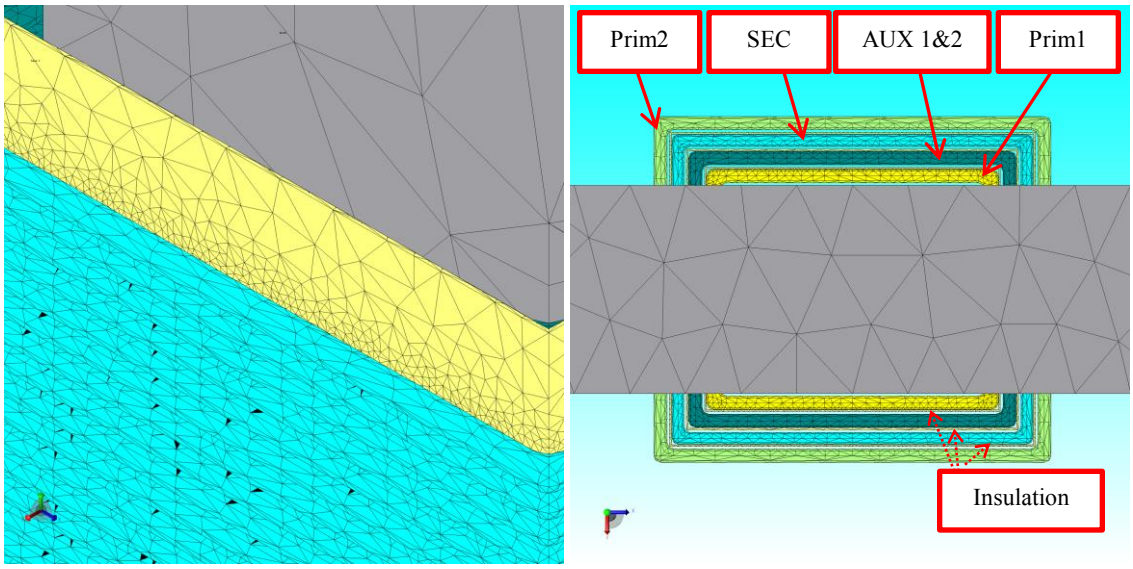

Figure 41: Mesh view of the model

The electrostatic analysis gives us the abilities to view contour plots of the model such as the electric potential and electric field. Figure 42 shows the electric potential contour plot of the model for determination the winding-to-winding capacitances in particular the AUX to Prim2 parasitic capacitance.

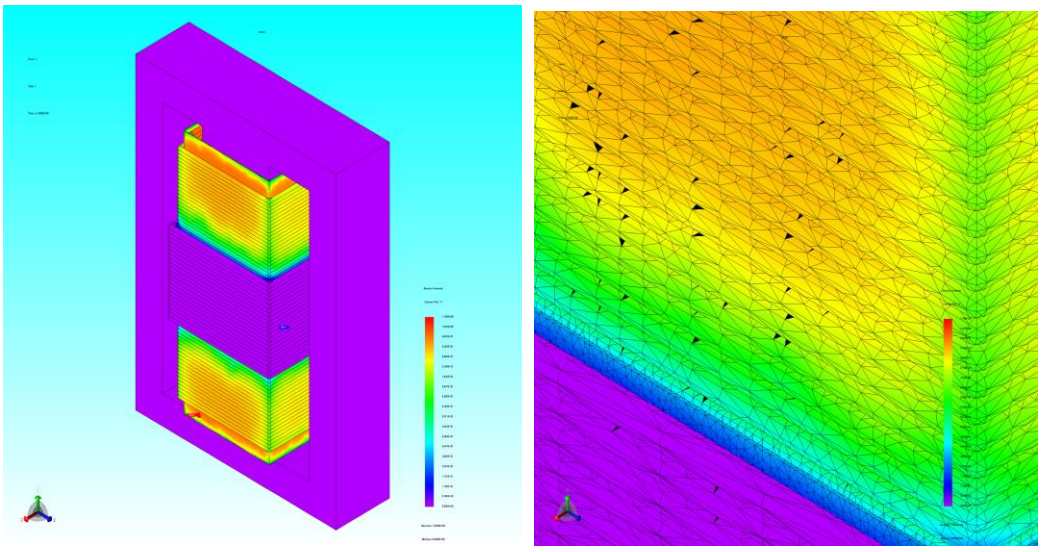

Figure 42: Electric potential contour plot for determination the AUX-Prim2 winding-to-winding capacitance

5.4 Prototype results and comparison

Table 9 shows the summary of the simulation results and experimental results. The comparison of simulation and experimental results shows good agreement. The percentages of error aren't unique for different parameters the bottommost error is 1.35% and the uppermost error is 7.58% for this case study.

Table 9: Summary of simulation and experimental results of prototype one

Parameter	Simulation	Experimental	% error
Self-Capacitance Prim1	332.66 PF	337.2 PF	1.35%
Self-capacitance Prim2	388.041 PF	399.2 PF	2.80%
Self-capacitance SEC	1023.13 PF	980.6 PF	4.34%
Self-capacitance AUX	1390.46 PF	1409.6 PF	1.36%
Prim1-Prim2	1021.019 PF	1000 PF	2.10%
Prim1-SEC	439.44 PF	420 PF	4.63%
Prim2-SEC	460.91 PF	440.4 PF	4.66%
Aux-SEC	340.16 PF	316.2 PF	7.58%
Aux-Prim2	333.41 PF	320.9 PF	3.90%
Aux-Prim1	298.9 PF	315.3 PF	5.20%

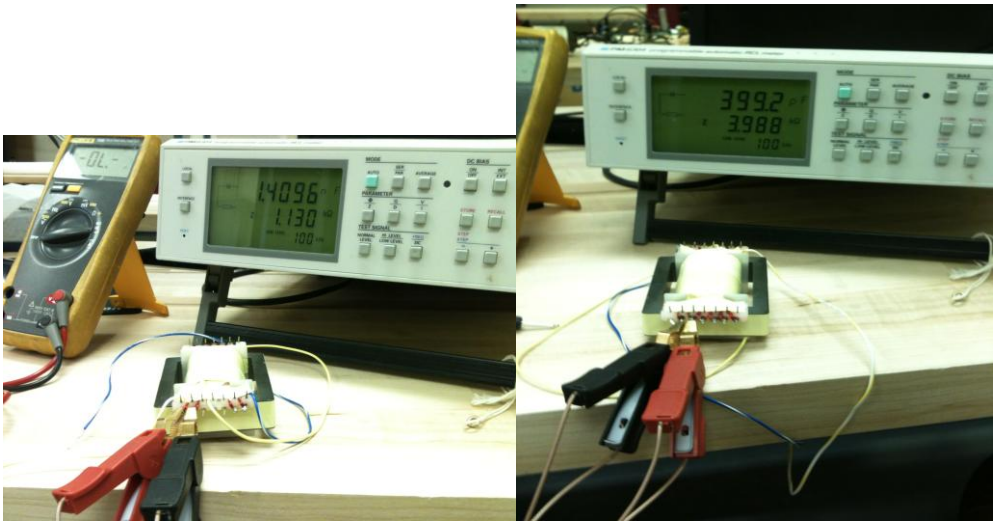

Figure 43: Experimental prototype

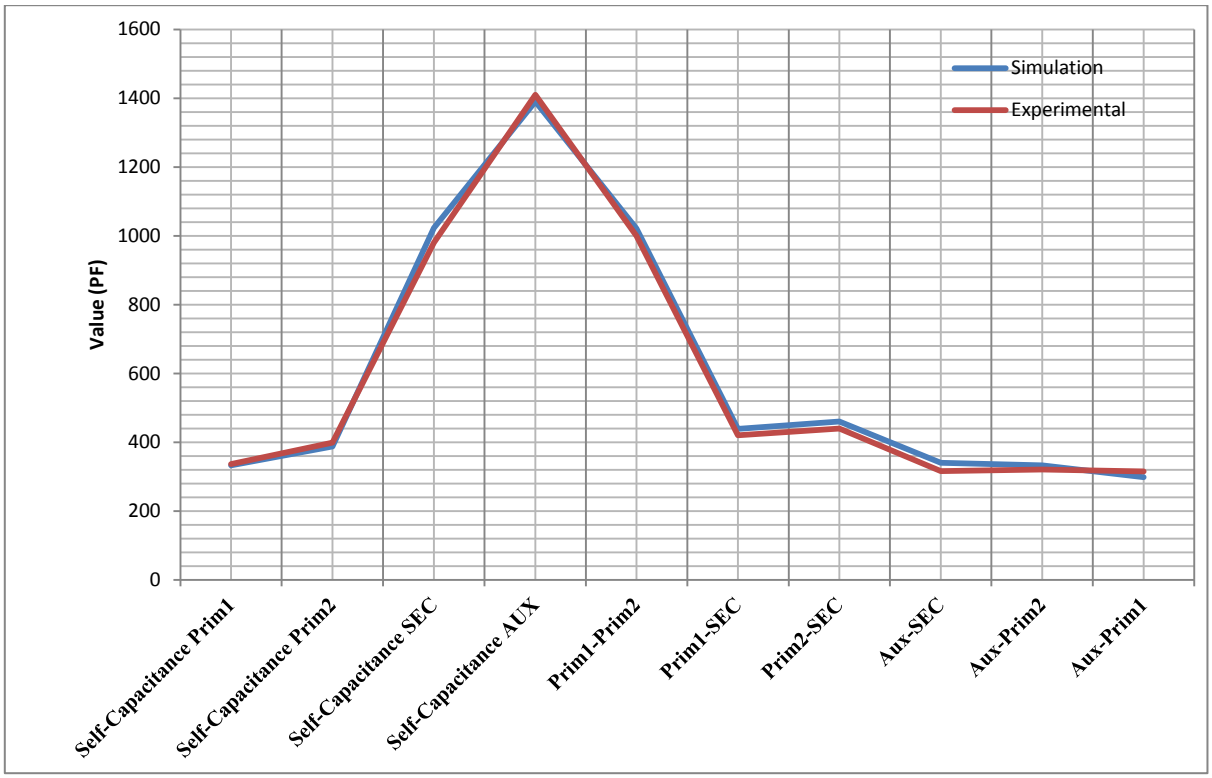

Figure 44: Simulation vs experimental results of prototype one

The simulation time for determination of self-capacitances is approximately 5 to 6 hours however it is higher for the inter-winding capacitances which is about 8 to 9 hours. Therefore the total time required for this prototype is approximately 68 hours by using a computer with Intel core 2 due processor and 4 GB of RAM. A possible way to reduce the simulation time is to do the parallel computing. Using several computers in parallel can reduce the simulation time significantly, JMAG reported that the number of computers using in parallel is proportional to the simulation time approximately.

6. FUTURE WORK

The main goal of this thesis was the determination of parasitic capacitances by means of FEA tool. Three different applications has been review as a case study. A possible future work of this thesis is the performance analysis of the switch mode power supplies (SMPS) including the parasitic parameters of the high frequency magnetic components. In addition to the discussed three applications mentioned in this thesis, the proposed methodology can be extended to determine the parasitic of switches using in SMPS.

The only non-linear part of magnetic components is the core. This thesis didn't cover the core saturation because the goal of this thesis is not to develop the core models. On the contrary, the main concern is the behavioral modeling of the winding at high frequency for using in SMPSs. This does not represent a serious limitation for the magnetic components in SMPSs because they work in linear region. Another extension work to this thesis is the development of the core models for in addition to the determination of parasitic capacitance of windings for use in other application which works in nonlinear region.

7. CONCLUSION

This thesis presented a comprehensive design-oriented frame work for calculating the parasitic capacitances of high frequency magnetic components. The analytical approach for determination of parasitic parameters in high frequency magnetics has been reviewed. A methodology for the calculation of intra- and inter-winding capacitances using the FEA tool JMAG has been demonstrated. The proposed methodology has been used in three different high frequency magnetic components for use in switching mode power supplies. The approach and formulas presented in this thesis can be applied to any other wound components. The proposed analysis of electrostatic behavior of high frequency magnetics is important for the following purposes:

- Reducing the design-prototype-test cycle time to couple of days which is traditionally a week from design to experimental test for multi-winding transformers in particular
- Utilization of the parasitic capacitance of transformers as an effective circuital parameter
- Reducing the capacitance value as an example by adjusting the winding arrangement
- Developing an approach of capacitance cancellation for instance in filter inductors [47]

Comparison of the simulation results with experimental results show good agreement. The main factors that are responsible for the error are the distance between the layers and the turn's arrangement.

Thus, this thesis propose a design-oriented framework to determine the parasitic capacitances of high frequency magnetics in switching power supplies using finite element analysis techniques.

REFERENCES

[1] R. Prieto, R. Asensi, C. Fernandez, and J. A. Cobos, "Bridging the gap between FEA field solution and the magnetic component model," in *IEEE Applied Power Electronics Conference and Exposition* (APEC), 2005, pp. 1315-1321 vol. 2.

[2] R. Prieto, R. Asensi, C. Fernandez, J. A. Oliver, and J. A. Cobos, "Bridging the Gap Between FEA Field Solution and the Magnetic Component Model," *IEEE Transactions on Power Electronics ,* vol. 22, pp. 943-951, 2007.

[3] J. Biela and J. W. Kolar, "Using transformer parasitics for resonant converters - a review of the calculation of the stray capacitance of transformers," in Record, *IEEE Industry Applications Conference, 2005*, pp. 1868-1875 vol. 3.

[4] F. S. Cavalcante and J. W. Kolar, "Small-Signal Model of a 5kW High-Output Voltage Capacitive-Loaded Series-Parallel Resonant DC-DC Converter," in *IEEE Power Electronics Specialists Conference* (PESC), 2005, pp. 1271-1277.

[5] L. Dalessandro, F. da Silveira Cavalcante, and J. W. Kolar, "Self-Capacitance of High-Voltage Transformers," *IEEE Transactions on Power Electronics,* vol. 22, pp. 2081-2092, 2007.

[6] A. Massarini and M. K. Kazimierczuk, "Self-capacitance of inductors," *IEEE Transactions on Power Electronics,* vol. 12, pp. 671-676, 1997.

[7] A. Massarini, M. K. Kazimierczuk, and G. Grandi, "Lumped parameter models for single- and multiple-layer inductors," in Record, *IEEE Power Electronics Specialists Conference* (PESC), 1996, pp. 295-301 vol. 1.

[8] X. Mao and W. Chen, "More precise model for parasitic capacitances in high-frequency transformer," in Record, *IEEE Power Electronics Specialists Conference* (PESC), 2002, pp. 1054-1057 vol. 2.

[9] A.V.D.Bossche and V.C.Valchev, *Inductors and Transformers for Power Electronics.* Boca Raton, FL: Taylor & Francis, 2005.

[10] M.K.Kazimierczuk, *High-Frequency Magnetic Components*, first ed. Singapore: J.Wiley, 2009.

[11] A. J. Palermo, "Distributed Capacity of Single-Layer Coils," in *Proceedings of the Institute of Radio Engineers,* vol. 22, pp. 897-905, 1934.

[12] H. Zuhrt, "Simple approximate formulas for the self capacitance of multi-layer coils,"in Record, *Elecktrotech. Zeitschrift,* vol. 55, pp. 662-665, Jul 1934.

[13] L. F. Casey, A. F. Goldberg, and M. F. Schlecht, "Issues regarding the capacitance of 1-10 MHz transformers," in *IEEE Applied Power Electronics Conference and Exposition* (APEC),1988, pp. 352-359.

[14] V. A. Niemela, G. R. Skutt, A. M. Urling, Y. N. Chang, T. G. Wilson, H. A. Owen, Jr., and R. C. Wong, "Calculating the short-circuit impedances of a multiwinding transformer from its geometry," in *IEEE Power Electronics Specialists Conference* (PESC), 1989, pp. 607-617 vol. 2.

[15] J. A. Collins, "An accurate method for modeling transformer winding capacitances," in *IEEE Industrial Electronics Society* (IECON), 1990, pp. 1094-1099 vol. 2.

[16] E. Laveuve, J. P. Keradec, and M. Bensoam, "Electrostatic of sound components: analytical results, simulation and experimental validation of the parasitic capacitance," in Record, *IEEE Industry Applications Society,*1991, pp. 1469-1475 vol. 2.

[17] P. Corsonello, P. Daponte, F. DeGrazia, and D. Grimaldi, "On two-coupled inductors stray capacitances evaluation for CAD-oriented modeling," in *Proceedings of Midwest Symposium on Circuits and Systems,* 1992, pp. 1252-1255 vol. 2.

[18] J. M. Lopera, M. Pernia, J. Diaz, J. M. Alonso, and F. Nuno, "A complete transformer electric model, including frequency and geometry effects," in *IEEE Power Electronics Specialists Conference* (PESC), 1992, pp. 1247-1252 vol. 2.

[19] L. Heinemann, R. Ullrich, B. Becker, and H. Grotstollen, "State space modeling of high frequency multiwinding transformers," in *IEEE Power Electronics Specialists Conference* (PESC), 1993, pp. 1091-1097.

[20] R. Asensi, J. A. Cobos, O. Garcia, R. Prieto, and J. Uceda, "A full procedure to model high frequency transformer windings," in *IEEE Power Electronics Specialists Conference* (PESC), 1994, pp. 856-863 vol. 2.

[21] A. Baccigalupi, P. Daponte, and D. Grimaldi, "On a circuit theory approach to evaluate the stray capacitances of two coupled inductors," *IEEE Transactions on Instrumentation and Measurement,* vol. 43, pp. 774-776, 1994.

[22] F. Blache, J. P. Keradec, and B. Cogitore, "Stray capacitances of two winding transformers: equivalent circuit, measurements, calculation and lowering," in Record, *IEEE Industry Applications Society*, 1994, pp. 1211-1217 vol. 2.

[23] B. Cogitore, J. P. Keradec, and J. Barbaroux, "The two-winding transformer: an experimental method to obtain a wide frequency range equivalent circuit," *IEEE Transactions on Instrumentation and Measurement,* vol. 43, pp. 364-371, 1994.

[24] R. Prieto, R. Asensi, J. A. Cobos, O. Garcia, and J. Uceda, "Model of the capacitive effects in magnetic components," in *IEEE Power Electronics Specialists Conference* (PESC), 1995, pp. 678-683 vol. 2.

[25] J. F. Charpentier, Y. Lefevre, and M. Lajoie-Mazenc, "A 2D finite element formulation for the study of the high frequency behaviour of wound components," *IEEE Transactions on Magnetics,* vol. 32, pp. 1098-1101, 1996.

[26] G. Grandi, M. K. Kazimierczuk, A. Massarini, and U. Reggiani, "Stray capacitances of single-layer air-core inductors for high-frequency applications," in Record*, IEEE Industry Applications Conference* (IAS), 1996, pp. 1384-1388 vol. 3.

[27] W. G. Hurley, W. H. Wolfle, and J. G. Breslin, "Optimized transformer design: inclusive of high-frequency effects," *IEEE Transactions on Power Electronics,* vol. 13, pp. 651-659, 1998.

[28] G. Grandi, M. K. Kazimierczuk, A. Massarini, and U. Reggiani, "Stray capacitances of single-layer solenoid air-core inductors,"in Record, *Industry Applications,* vol. 35, pp. 1162-1168, 1999.

[29] J. Pleite, R. Prieto, R. Asensi, J. A. Cobos, and E. Olias, "Obtaining a frequency-dependent and distributed-effects model of magnetic components from actual measurements," *IEEE Transactions on Magnetics,* vol. 35, pp. 4490-4502, 1999.

[30] M. J. Prieto, A. Fernandez, J. M. Diaz, J. M. Lopera, and J. Sebastian, "Influence of transformer parasitics in low-power applications," in *IEEE Applied Power Electronics Conference and Exposition* (APEC), 1999, pp. 1175-1180 vol. 2.

[31] A. Schellmanns, J. P. Keradec, J. L. Schanen, and K. Berrouche, "Representing electrical behaviour of transformers by lumped element circuits: a global physical approach," in Record, *IEEE Industry Applications* (IAS), 1999, pp. 2100-2107 vol. 3.

[32] T. Duerbaum, "Capacitance model for magnetic devices," in *IEEE Power Electronics Specialists Conference* (PESC), 2000, pp. 1651-1656 vol. 3.

[33] L. Heinemann and J. Helfrich, "Modeling and accurate determination of winding losses of high frequency transformers in various power electronics applications," in *IEEE Applied Power Electronics Conference and Exposition* (APEC), 2000, pp. 647-653 vol. 2.

[34] H. Y. Lu, J. G. Zhu, and V. S. Ramsden, "Comparison of experimental techniques for determination of stray capacitances in high frequency transformers," in *IEEE Power Electronics Specialists Conference* (PESC), 2000, pp. 1645-1650 vol. 3.

[35] L. Hai Yan, Z. Jian Guo, and S. Y. R. Hui, "Experimental determination of stray capacitances in high frequency transformers," *IEEE Transactions on Power Electronics,* vol. 18, pp. 1105-1112, 2003.

[36] J. M. Lopera, M. J. Prieto, A. M. Pernia, and F. Nuno, "A multiwinding modeling method for high frequency transformers and inductors," *IEEE Transactions on Power Electronics,* vol. 18, pp. 896-906, 2003.

[37] Z. Jun, C. Qianhong, R. Xinbo, W. Siu Chung, and C. K. Tse, "Experimental measurement and modeling of multi-winding high-voltage transformer," in *Inter Conf on Electrical Machines and Systems* (ICEMS), 2008, pp. 4411-4415.

[38] M. B. Shadmand and R. S. Balog, "FEA Tool Approach for Determination of Parasitic Capacitance of the Windings in High Frequency Coupled Inductors Filters," in *IEEE Power and Energy Conference at Illinois* (PECI), Urbana, Illinois, Feb 2012.

[39] M. B. Shadmand and R. S. Balog, "Determination of Leakage Inductance and Self Capacitance of the Windings in a High Frequency Switching Power Supply Inductors Using JMAG," in *IEEE Applied Power Electronics Conference and Exposition* (APEC), submitted for peer review-Rejected.

[40] M. B. Shadmand and R. S. Balog, "Determination of Parasitic Parameters in a High Frequency Magnetic to Improve the Manufacturability, Performance, and Efficiency of a PV Inverter," in *IEEE Photovoltaic Specialist Conference*, Austin, Texas, to appear, Jun 2012.

[41] M.K. Kazimierczuk, *High-Frequency Magnetic Components*, first ed. Singapore: J.Wiley, 2009.

[42] W. Shuo, F. C. Lee, and J. D. van Wyk, "Inductor winding capacitance cancellation using mutual capacitance concept for noise reduction application,"

IEEE Transactions on Electromagnetic Compatibility, vol. 48, pp. 311-318, 2006.

[43] R. S. Balog and P. T. Krein, "Coupled Inductor Filters: A Basic Filter Building Block," *IEEE Transactions on Power Electronics,* accepted for publication, Jan 2011.

[44] R. S. Balog, "Coupled Inductor : A Basic Filter Building Block: Analysis, Simulation, and Examples," MS Thesis, Department of Electrical and Computer Engineering, University of Illinois at Urbana-Champaign, 2002.

[45] R. Balog and P. T. Krein, "Automatic tuning of coupled inductor filters," in *IEEE Power Electronics Specialists Conference* (PESC), 2002, pp. 591-596 vol. 2.

[46] M. Alizadeh B, H. Khomami P, and M. Rajabzadeh, "New design and implementation of an external passive circuit for cancelling the parasitic capacitance in filter inductors," in *Joint International Conference on Power Electronics, Drives and Energy Systems* (PEDES), 2010, pp. 1-4.

[47] T. C. Neugebauer and D. J. Perreault, "Parasitic capacitance cancellation in filter inductors," *IEEE Transactions on Power Electronics,* vol. 21, pp. 282-288, 2006.

[48] R. Prieto, J. A. Cobos, O. Garcia, and J. Uceda, "Interleaving techniques in magnetic components," in *IEEE Annual Applied Power Electronics Conference and Exposition* (APEC), 1997, pp. 931-936 vol. 2.

[49] H. A. Owen, Jr., V. A. Niemela, and T. G. Wilson, "Enhanced cross-coupled-secondaries model for multiwinding transformers," in *IEEE Power Electronics Specialists Conference* (PESC), 1992, pp. 1269-1276 vol. 2.

[50] R. Prieto, J. A. Cobos, O. Garcia, P. Alou, and J. Uceda, "High frequency resistance in flyback type transformers," in *IEEE Applied Power Electronics Conference and Exposition* (APEC), 2000, pp. 714-719 vol. 2.

[51] A. F. Witulski, "Introduction to modeling of transformers and coupled inductors," *IEEE Transactions on Power Electronics,* vol. 10, pp. 349-357, 1995.